RESPONSES TO REQUESTS FOR ADDITIONAL INFORMATION

LICENSE AMENDMENT REQUEST 226

MEASUREMENT UNCERTAINTY RECAPTURE POWER UPRATE

POINT BEACH NUCLEAR PLANT, UNITS 1 AND 2

Attachment 3

MPR Associates, Inc. Engineering Report MPR-1619,

Rev. 0, Appendix B (Non-Proprietary Version)

MPR Associates, Inc.
Engineering Report: MPR-1619, Rev. 0

Feedwater Flow Measurement with LEFM Chordal Systems at Point Beach Units 1 and 2

Configuration and Uncertainty Analysis

Appendix B

(Non-Proprietary Version)

MPR

MPR Associates, Inc.
320 King Street
Alexandria, VA 22314

CALCULATION TITLE PAGE

Client Caldon, Inc.	Page 1 of 14
Project Point Beach LEFM Uncertainty Analysis	Task No. 157-076
Title Hydraulic Profile and Its Uncertainty - Unit 1	Calculation No. 157-076-SKK-01

Preparer/Date	Checker/Date	Reviewer/Date	Rev. No.
Son Kim SON KIM 5/16/95	Matthew E. Roberts Matthew E. Roberts 5/16/95	D. E. Magnola D. E. Magnola 5/16/95	0

MPR

MPR Associates, Inc.
320 King Street
Alexandria, VA 22314

RECORD OF REVISIONS

Calculation No.	Prepared By	Checked By	Page 2
157-076-SKK-01			

Revision	Description
0	Original Issue

TABLE OF CONTENTS

1.0 PURPOSE

The Leading Edge Flow Meter (LEFM) calculates volumetric flow from fluid velocity measurements along acoustic paths in a measurement section or spool piece. The relationship between the velocity measured along the acoustic paths and the volumetric flow is determined by (a) the angle between the acoustic paths and the axial fluid velocity vectors which intersect them and (b) a profile factor which relates the axial velocities along the acoustic paths to the axial velocity averaged over the cross section of the spool piece. This calculation provides the basis for the profile factor to be used with the four-path chordal flow meter installed at Point Beach Unit 1, and calculates the uncertainty bounds on the profile factor.

2.0 SUMMARY

A profile factor of [ ] should be used with the four-path chordal flow meter at Point Beach Unit 1, and the uncertainty in this profile factor is [ ].

3.0 APPROACH

The profile factor and its accuracy for a four-path chordal flow meter are dependent upon the ability of the meter to integrate from discrete velocities measured on each of four paths into the spatially averaged velocity across the spool piece section. This integration is affected by the inaccuracy of the four path Gaussian Quadrature integration method, and the fact that the velocity profile is not uniform across the section. The velocity profile is non-uniform on two counts. First, in long straight sections of pipe the velocity profile becomes rounded, blunt and symmetrical, characterized as "fully developed". In a fully developed profile (Figure 1), the velocity has a maximum at the fluid center and minimum at the pipe wall. Secondly, actual piping systems like the Point Beach feedwater system contain bends and other fittings which produce, in varying degrees, asymmetrical distortions that change the velocity gradients and introduce secondary non-axial flows.

To estimate the Point Beach Unit 1 four-path chordal profile factor and its uncertainty, this calculation takes the following approach:

(1) [

]

(2) [

]

[

]

(3) [

]

4.0 CALCULATION

4.1 Profile Factor and Uncertainty for Fully Developed Turbulent Flow

Reference 1 establishes a profile factor versus Reynolds Number for measurement of fully developed flow using a four-path chordal flow meter. [

]

4.2 Point Beach Unit 1 Hydraulic Geometry Effects

The piping arrangement and flow meter orientation in the Point Beach Unit 1 feedwater piping are sketched in Figure 2 (Reference 2). The flowmeter is located in a straight run of horizontal piping approximately 31 pipe diameters downstream of an elbow. In turn, the elbow is approximately 2 diameters downstream of a converging tee. One of the lines feeding this tee is perpendicular to the plane of the elbow. A converging tee is also located in the straight run of horizontal piping 17.5 pipe diameters upstream of the LEFM. However, the line feeding this tee is a bypass line which is normally closed. No additional hydraulic effect is anticipated.

[

]

[

]

Murakami has extensively tested non-coplanar bends. Murakami's data shows that a swirl, once created may persist for up to 150 pipe diameters. On the basis of Murakami's data, the swirl should be detectable at the LEFM location 31 diameters from the elbow. Evaluation of the LEFM in-situ path velocity data confirms the presence of a swirl in the expected direction.

Figure 2 shows the orientation and numbering of the LEFM paths at Point Beach Unit 1. Individual path velocities recorded during commissioning of the LEFM at Point Beach Unit 1 are summarized in Table 1 below, for which the following nomenclature applies:

[

]

[

]

[ ]

4.3 Velocity Profile Asymmetry Effects

All four of the LEFM acoustic paths measure the fluid velocity in the same spatial plane. Accordingly, asymmetries in the velocity profile have the potential to cause measurement error. In the case of Point Beach Unit 1, the potential sources of asymmetry in the velocity profile are:

- Axial velocity profile asymmetry due for example to the upstream bend, misalignment of the LEFM spoolpiece with the upstream pipe, or variations in pipe roughness.
- [ ]

[ ]

[

]

[

]

4.4 Combination of Errors

- [ ]
- [ ]
- [ ]
- [ ]
- [ ]

[ ]

5.0 REFERENCES

1. MPR Calculation Number 15708HE1A, "Determination of the Profile Factor and Its Uncertainty for a 4 Path LEFM in Long Straight Pipe," Rev. 0, H. Estrada, 12/18/82.

2. Bechtel Drawing No. P-121, Rev. 4 (Job No. 10447), "Boiler FW Pumps to CTMT Isolation Valve (DB-1), Unit 1."

3. Murakami, M., Shimizu, Y., and Shiragumi, H., "Studies on Fluid Flow in Three Dimensional Bend Conduits," Japan Society of Mechanical Engineers (JSME) Bulletin V. 12, No. 54, Dec. 1969, pp 1369-1379.

4. Caldon Procedure No. EFP56, "Commissioning Procedure for LEFM 8300 Wetted Transducer Single Plane Chordal System," Completed 4/27/95 for Point Beach Unit 1 Installation by M. Brink (Caldon) and M. Roberts (MPR).

5. MPR Calculation Number 108-054-LAS-03, Rev. 0, "Average Chordal Velocities for Universal Fluid Velocity Model."

6. MPR Calculation Number 157-076-SKK-02, Rev. 0, "Effect of LEFM Chordal Path Orientation on Measured Profile Factor".

7. Abernathy et al, "ASME Measurement Uncertainty," ASME Journal of Fluids Engineering, Vol. 107, p. 161-164, June 1985.

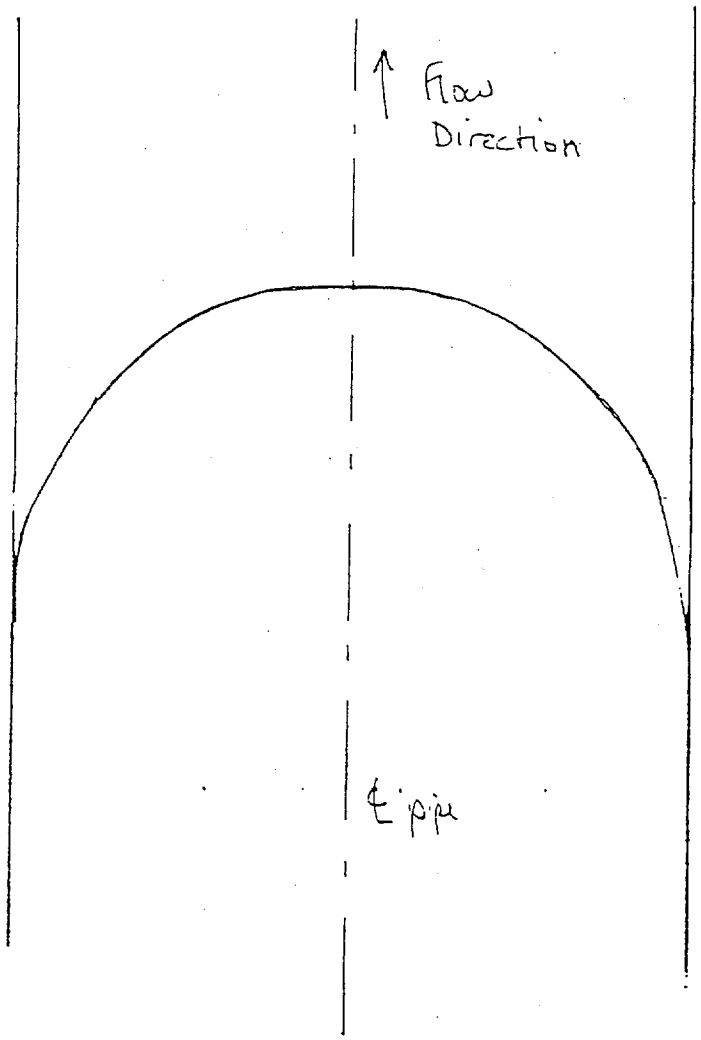

FIGURE 1

Fully Developed Flow Profile (Typical)
(Turbulent)

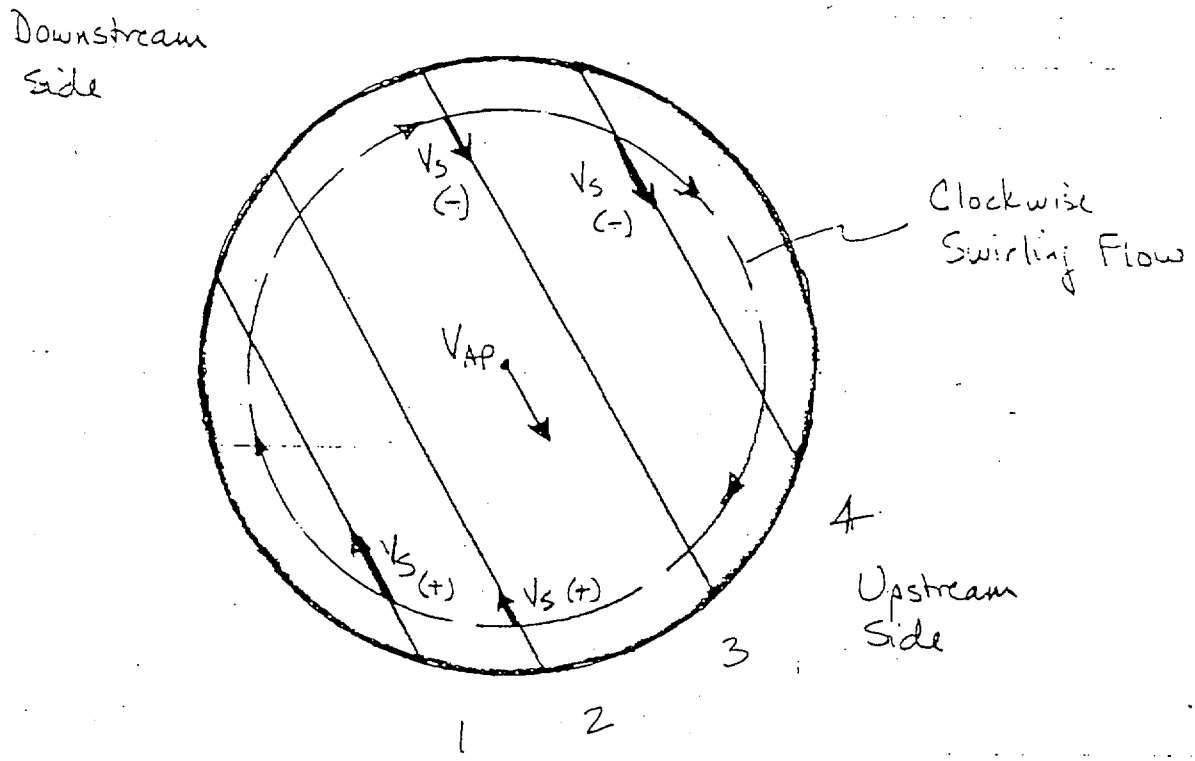

V_{AP} = Direction of Axial Flow Projected on All paths

FIGURE 3

Effect of Axisymmetric Swirl on LEFM Path Velocities

Japan Society of Mechanical Engineers (JSME), Bulletin, vol. 12, no. 54, Dec. 1969, pp. 1369-1379.

Attachment 1

532.542 : 532.55

Studies on Fluid Flow in Three-Dimensional Bend Conduits*

By Mitsukiyo MURAKAMI**, Yukimaru SHIMIZU***, and Heiji SHIRAGAMI****

This paper gives the results of the experimental study of loss and secondary circulation due to various combinations of commercial elbows, and discussed the relationship between the loss and the circulation. Three general combinations are: One where the two elbows produce a complete reversal in the direction of flow, termed the "U" bend; and two where the two elbows produce an offset but no change in direction, termed the "S" bend; and three where the two elbows produce both an offset and a 90 degree change in the direction of flow, termed the "twisted S" bend.

The last combination gives rise to a strong single spiral motion in the straight pipe of curved pipes downstream and shows the maximum bend loss.

1. Introduction

A pipe line of a fluid machine or other hy-lic plants has often many complicated curved ions. When a fluid flows through such a curv-ipe, the fluid acquires a secondary flow com-t, which would not present itself in a straight flow. The secondary flow produces an addition-ydraulic loss. Particularly when two curved are located in different planes, a strong spiral n is produced in the pipe and the distribution e exit velocity is deformed remarkably, result-a great loss. When the fluid enters a fluid ne or a flow meter with the deformed veloc-: alters their performances considerably.

Many studies[1]-[11] on this subject have been in the past, but the most of them concern he hydraulic loss on smooth bends having a ely larger radius of curvature. A right-angled rcial elbow has a relatively small bend and also a sudden contraction or enlargement sections of screw joints, which complicates w patterns and prohibits a theoretical ap-

e object of this paper is to clarify experi-y the relationship between hydraulic loss and distribution of two elbows located succes-n a pipe line.

eceived 27th July, 1966.

rofessor, Faculty of Engineering, Nagoya Univer-y.

sistant, Faculty of Engineering, Nagoya University, ikusa-ku, Nagoya.

gineer, Mitsubishi Heavy Industry Co.

2. Nomenclature

d: diameter of pipe

g: acceleration of gravity

H: total loss of head in gauge length

L_d: distance of downstream pressure tap (section 9 in Fig. 2) from exit of the second elbow

L_m: length of spacer between the first and the second elbows

L_u: distance of upstream pressure tap (section 0 in Fig. 2) from entrance of the first elbow

L: $L_d+L_m+L_u$, total gauge length

r: radial distance

R: radius of pipe

p_1: static pressure at section 0 in Fig. 2

p_2: static pressure at section 9 in Fig. 2

p_i: wall pressure at any section downstream from the second elbow

V_z: axial component of velocity

V_{zmax}: maximum value of V_z

V_θ: tangential component of velocity

$V_{\theta max}$: maximum value of V_θ

V_m: mean velocity calculated from orifice readings

γ: specific weight of water

ρ: radius of curvature of curved pipe

ζ: coefficient of total loss due to two elbows as defined by Eq. (1)

ζ_1: coefficient of apparent total loss due to two elbows, calculated by Eq. (1) with p_1 and p_i

ζ_0: coefficient of loss due to a single elbow in a pipe line

λ: friction factor for straight pipe

ψ: angle of pipe line twisted by two elbows, as defined by Fig. 3

Notations in Fig. 3

N-plane: plane normal to bend surface of the second elbow

P-plane: bend plane of the second elbow

Suffix

N: normal direction to P and Z and on N-plane

P: normal direction to N and Z and on P-plane

Z: downstream direction along pipe line.

3. Experimental apparatus and procedure

The general arrangement of the test apparatus is indicated in a schematic diagram, Fig. 1. A steady pressure was maintained in the metering system by a head tank for low-pressure range and by a centrifugal pump for high-pressure range. A flexible pipe was employed to facilitate the bend configuration of pipe line. The flow rate of the piping system was measured by an orifice meter. The measuring pipes 6, 8, and 10 are of brass and the inside diameters are 53.75, 53.84, and 53.90 mm respectively, and the pipes have hydraulically smooth surface. The details of measuring pipes are shown in Fig. 2. Distance of two elbows, namely, the spacer length and an angle of twist of pipe line used in this experiment are given in Table 1. Each measuring section has four taps, the diameter of which is 1 mm and equally spaced circumferentially. The upstream section 0 is located 35 pipe diameters downstream from the rectifying tank to eliminate the effects of the inlet length*. The measuring section 9 downstream from the second elbow is selected at the position where the effect of elbows disappears. Depending on the twisted angle ψ and the length of spacer L_m, the position of the section changes from 150 to 300 diameters downstream from the second elbow. The position was selected on the basis of pressure distribution along the pipe line and velocity profiles of the pipe sections.

To avoid an error due to fluctuation of manometer readings, a rotary cock is inserted in all the pressure transmitting pipes from taps to manometers. After closing the cock, the manometer readings were taken. A cylindrical pitot tube with three holes was traversed in the sections shown by dotted lines a~h in Fig. 2 and velocity profile was obtained (tube diameter=3.025 mm, hole diameter=0.3 mm). To check the accuracy of measurements, the flow quantity evaluated by a graphical integration of axial component of velocity was compared with that by the orifice meter. The difference was proved to be less than 5 percent.

Coefficient of the total fitting loss due to two elbows located in series in a pipe line is calculated by the following equation:

$$H=\frac{p_1-p_2}{\gamma}=\lambda\left(\frac{L}{d}\right)\left(\frac{V_m^2}{2g}\right)+\zeta\left(\frac{V_m^2}{2g}\right) \quad \cdots\cdots\cdots\cdots (1)$$

Table 1 Length of spacer L_m/d and angle of turn ψ of pipe line employed in this test

L_m/d	0	0.65	2.15	4.7	9.8		
ψ	0°	45°	90°	120°	135°	140°	180°

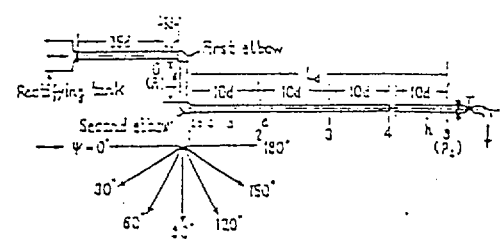

1~9 : Measuring sections of pressure
a~h : Measuring sections of velocity
a : 0.1 d from the second elbow
b : 0.5 d
c : 3 d
h : (150~250) d

Fig. 2 Measuring sections and angle of turn of pipe line

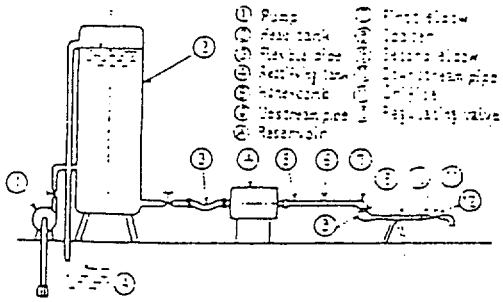

Fig. 1 Schematic diagram of test arrangement

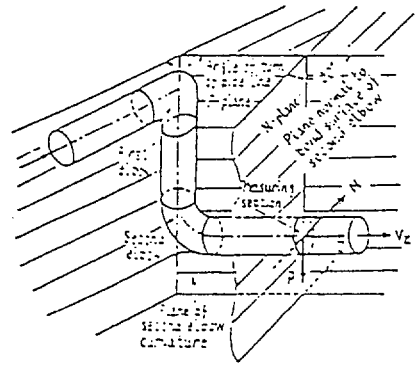

Fig. 3 Definition of sections and directions

* The effects of the inlet length on ζ are negligible when the length ranges from 5 to 35 pipe diameters.

hen a single elbow is in a pipe line, the loss coef-
ent ζ in Eq. (1) reduces to ζ_0, the loss coefficient
to a single elbow.

4. Experimental results and discussion

4·1 Loss of head by two 90-degree elbows

Hydraulic losses due to combination of two
bows have been studied by many investigators.
ut knowledges of the distortion of velocity at the
end exits and its relations with the hydraulic loss
e not sufficient. In the following, results of this
periment on head loss due to bends are summariz-
and compared with those obtained by the other
vestigators.

4·1·1 Pipe length required to recover normal tribution of velocity

Due to generation of a secondary flow by pipe
nds, distributions of velocity and pressure in a
e section downstream from the bends are distort-
considerably. The secondary flow decays toward
vnstream and the distortion of the velocity is
dually recovered to the normal flow conditions.
is, by examining the pressure drop along the
downstream from the second elbow, position of
nearest section at which the normal flow con-
ons will be re-established can be found.

In Fig. 4 apparent coefficient of loss ζ_1 by Eq.
is plotted against L_d/d, where the wall pres-
p_1 downstream from the second elbow is used
in place of p_1. As the measuring section of p_1 is kept
away from the second elbow, ζ_1 tends to a constant
value, i.e. the true fitting loss of the bend ζ.
Apparently, by introducing a short length of a pipe
L_m, namely a spacer, between the two elbows, the
value of bend loss ζ is altered. For reference,
results of a single elbow in a pipe line are also
plotted. In this case, ζ reaches a constant value
of 0.735, the true loss coefficient, when the wall
pressure p_1 at section of $L_d=50\,d$ is used. When
two elbows are located in U ($\psi=0°$) and S ($\psi=$
180°) forms in the same plane, ζ_1 flattens off in a
shorter length. When two elbows are off set in the
twisted S form, for example $\psi=120°$ and 140°, the
turned effects extend as far as $L_d=160\,d$. The above
results show that the required pipe length in which
the turned effect disappears from the pipe line will
be much altered by the turned form. Table 2 gives
this required pipe length, which is unaffected by
Reynolds number in this experimental range.

4·1·2 Coupling depth of screw joint and hydraulic loss

The coupling depth of a screw joint between an
elbow and a pipe has a considerable effect on the
fitting losses of the elbow. Figure 5 shows the
results of experiments, where the two elbows are
located in S form in the same plane. Depending
upon the coupling condition of screw joints the fit-
ting loss is seen to be scattered about 15 percent.
Throughout this paper, with exception of the pre-
sent section, the loss of elbows is referred to the
case when the pipe ends are fully screwed to the
coupling parts.

4·1·3 Effects of twisted angle ψ and spacer length L_m between two elbows on turned loss

Figure 6 shows the relation between ζ and ψ
for various values of L_m/d. With small value of
L_m/d, ζ is much affected by ψ. From a minimum
value of $\psi=0°$, ζ increases and takes a maximum

. 2 Minimum pipe length L_d behind the second elbow to recover normal flow conditions

L_m/d \ ψ	0°	45°	90°	135°	180°
0	($\psi=3°$) 45	100	180	180	45
55	($\psi=2.5°$) 45	110	160	160	80
7	50	60	80	80	80

Far very short spacer length L_m/d of 0 and 0.65, pipe line can not be turned strictly U-shape.

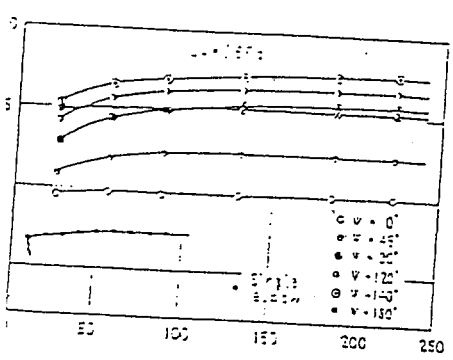

Fig. 4 Curves for ζ_1-L_d/d

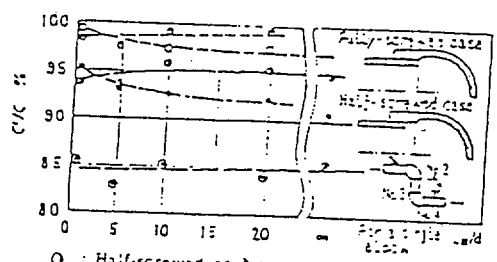

O : Half-screwed at No. 1 only
C : Half-screwed at No. 2 only
O : Half-screwed at No. 3 only
● : Half-screwed at No. 4 only
⊕ : Half-screwed at all joints
ζ' = Loss coefficient in Half-screwed case
ζ = Loss coefficient in Fully-screwed case

Fig. 5 Relation between screwed depth of joints and loss coefficients

value at about $\psi=130°\sim140°$, and again it decreases to the value of $\psi=180°$. For reference, twice the loss of a single elbow, $2\zeta_0$, is shown in Fig. 6. When length of the spacer L_m is less than $4.7\,d$, ζ has a maximum and it exceeds the value $2\zeta_0$ at an angle $\psi=80°$. When $L_m=4.7\,d$, the maximum value becomes less than $2\zeta_0$ and is changed by the twisted angle ψ of pipe line. When $L_m\geqq10\,d$, ζ is independent of the angle ψ and remains constant. The value, however, is appreciably less than twice the single elbow loss, $2\zeta_0$, exhibiting an existence of interference of elbows. Even with this interference, loss of the combined elbows is independent of the twisted angle. The reason is clarified by examining the velocity profile downstream from the first elbow. The velocity is seen to be distributed nearly in axial symmetry but is not fully developed, the details of which will be described later.

In the past, several investigators[7, 10, 11] have measured the turned loss of two bends combined and they all observed an existence of a maximum loss at about an angle $\psi=90°$, and the value was always less than twice the single elbow loss, $2\zeta_0$, the results being different from the above. The reason will probably be attributable to the fact that the past experiments were made with smooth curved pipes having a larger radius of curvature ($\rho/d\geqq2$).

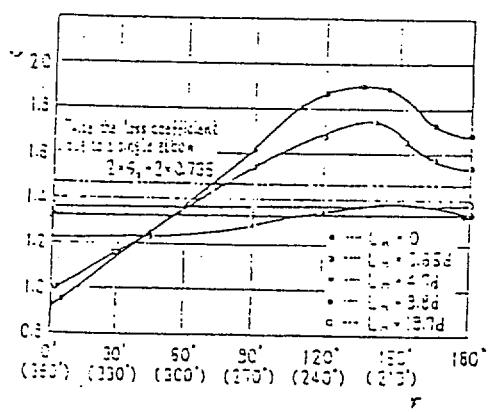

Fig. 6 $\zeta-\psi$

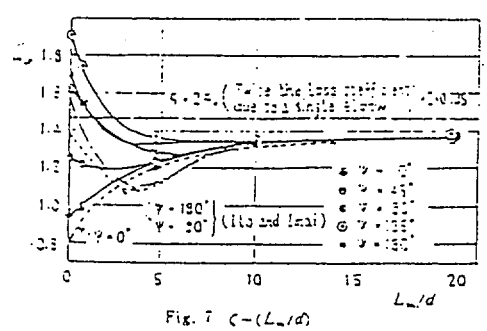

Fig. 7 $\zeta-(L_m/d)$

Relation between ζ and L_m/d is plotted for several values of ψ in Fig. 7, where Ito's data[11] are also given. ζ changes sharply within the small range of $L_m/d<5$. When ψ is less than 45°, ζ increases with L_m, but when $\psi\geqq45°$, ζ decreases to one minimum value and again increases as L_m is increased. In all cases, the loss mentioned the above are proved to be unaffected by Reynolds number in this experimental range and hence its descriptions are omitted. However, when the pipe line is bent three-dimensionally with an angle $\psi=90°\sim180°$, and the length of spacer L_m is reduced to zero, a few percentage variations of the turned loss is seen by change of Reynolds number.

4·2 Distribution of velocity

4·2·1 Single curved pipe (with one elbow)

Due to sudden enlargements or contractions in elbow joints, the flow pattern is much disturbed and

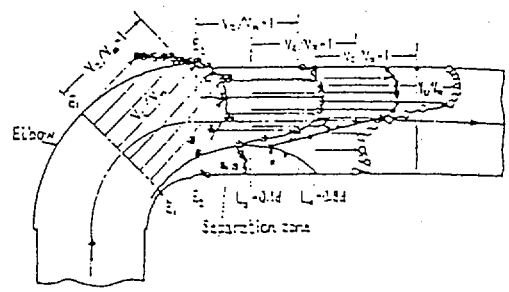

(a) Distribution of axial velocity in bend plane (N-plane), (Single elbow)

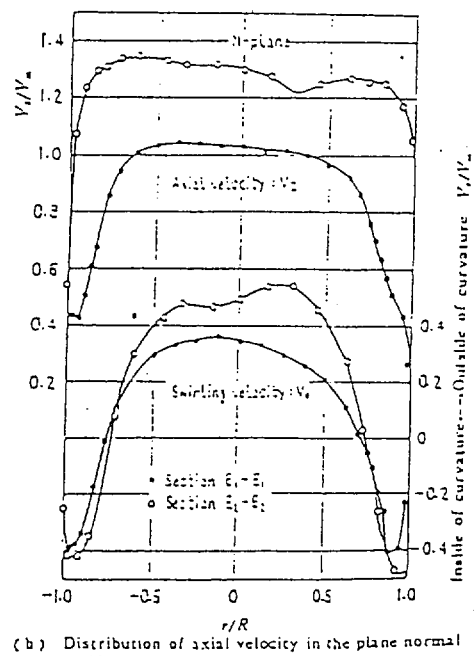

(b) Distribution of axial velocity in the plane normal to N-plane

Fig. 8

curate measurements of velocity distribution in e elbow will encounter great difficulty. Figure 8) and (b) show velocity profiles in an elbow. the middle section E_1-E_1 of the elbow, Fig. 8(a), gher velocity is observed inside the curvature, the w resembling a free vortex motion. The axial locity on N-plane, Fig. 8 (b), of the same sec- on has nearly an even distribution. On the other hand, a fairly intensive secondary flow is set up in this section. As a result, the maximum axial velocity is further displaced from the centre of pipe towards the outer wall. Thus a considerable elevation of the axial velocity is seen near the outer wall. At the same time, the flow velocity near the centre is reduced gradually, resulting in a concave velocity profile, N-plane. In addition, sharp bend

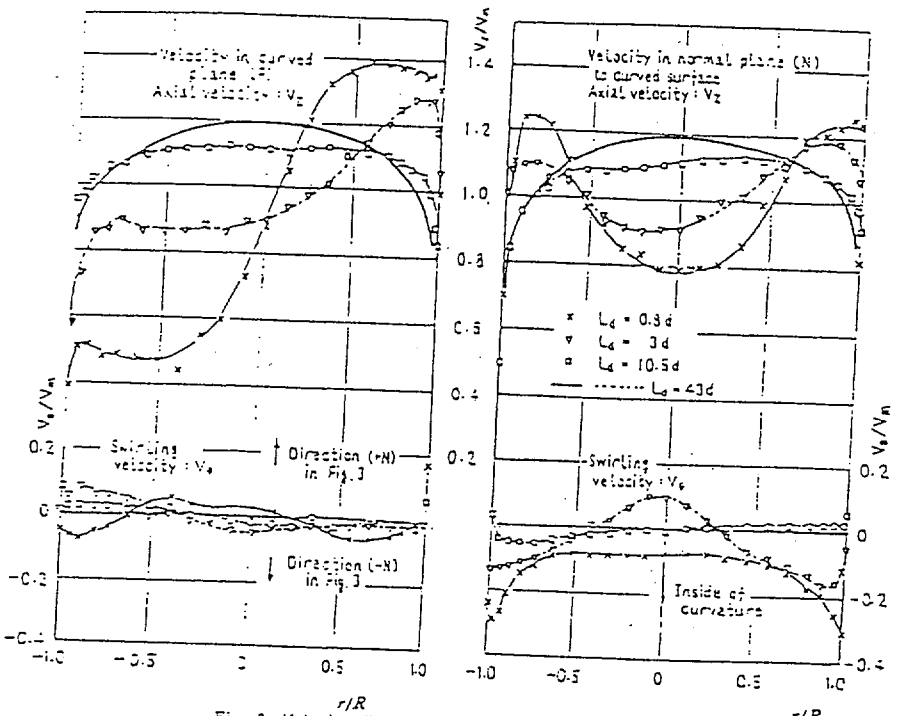

Fig. 9 Velocity distribution downstream from a single elbow

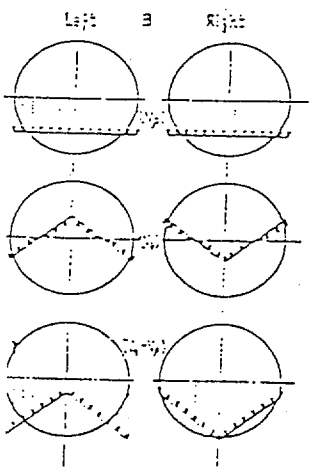

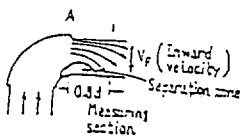

B. Left : velocity profile at $L_d = 0.8\,d$ (single elbow)
B. Right : velocity profile at $L_d = 0.8\,d$ (two elbows combined)
(1) Inward velocity, Fig. A: (V_F)
(2) Ordinary type of secondary flow (V_s)
(3) Combination of (1) and (2) : ($V_s + V_F$)

Explanation of abnormal type of secondary flow behind elbows

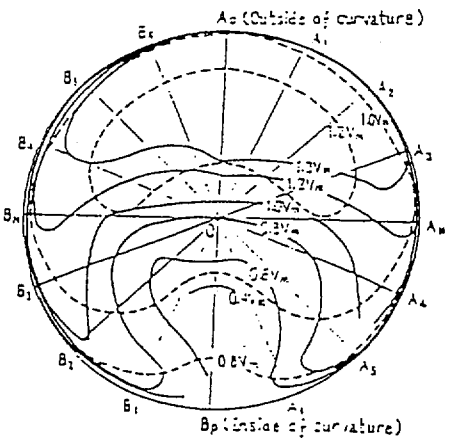

— Present Test, $p/d = 1$, $R_e = 10^4$
— Adler, $p/d = 100$, $R_e = 1.17 \times 10^4$

Fig. 11 Equi-velocity lines at $L_d = 0.8d$, (V_s)

of the elbow develops a flow separation at the inner wall of the section E_1-E_1, which accentuates the uneven distribution of axial velocity. Thus, a maximum displacement of the axial velocity occurs near the section $L_s=0.1\,d$, just after the elbow exit, and after the section the velocity is recovered gradually to that of the normal flow condition, Fig. 9. An abnormal type of secondary flow is seen at section $L_s=0.8\,d$, where all of the fluids in N-plane move inwards of the curvature. The reason why this type flow occurs can be studied on a simple model as shown in the left of Fig. 10. The ex-

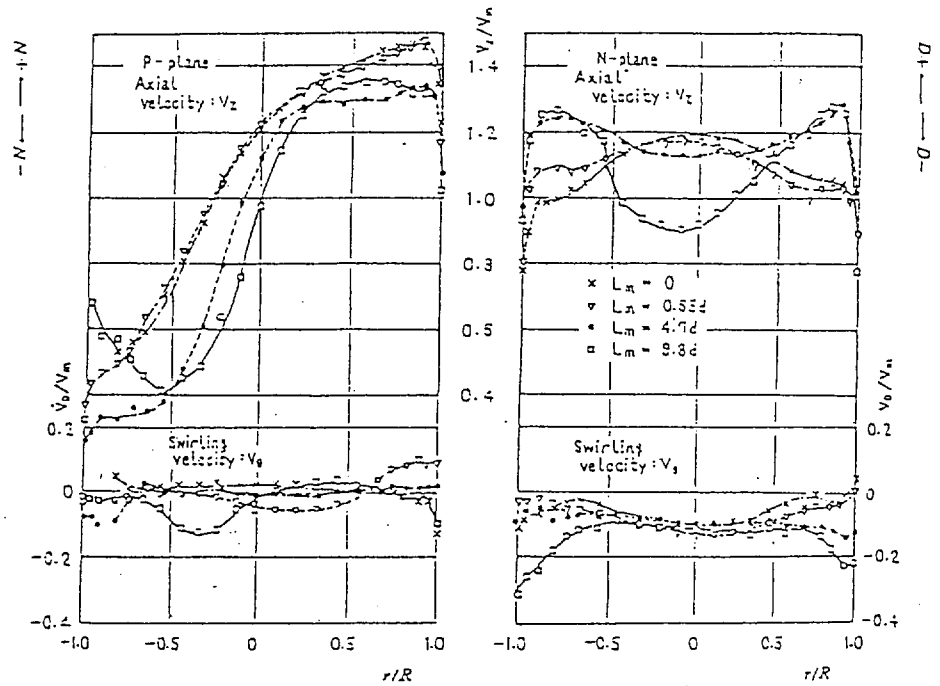

Fig. 12 Relation between velocity profile at $L_s=0.8\,d$ and L_m ($\psi=0°$)

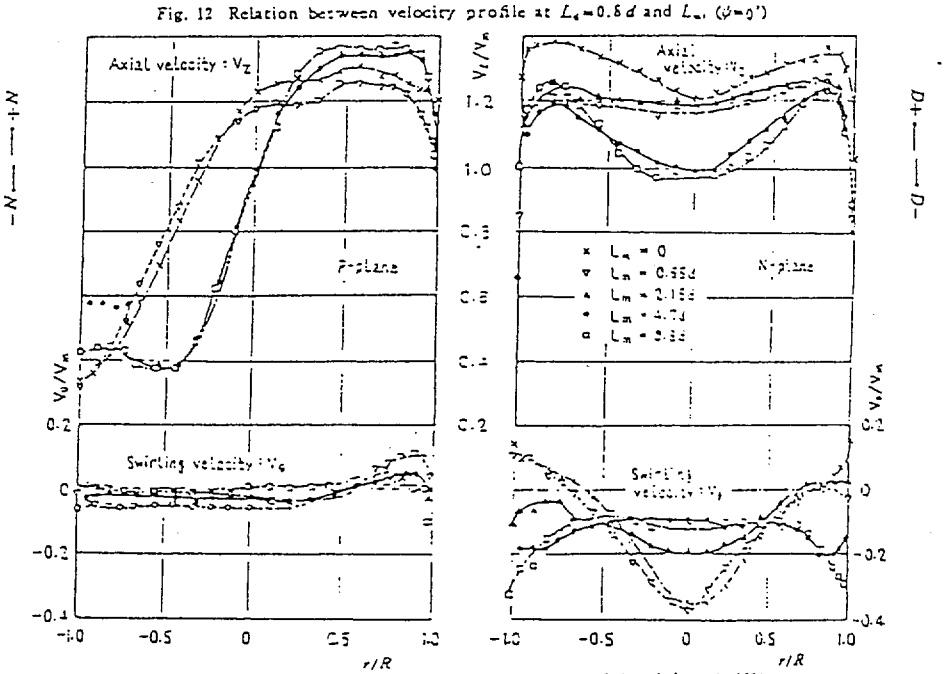

Fig. 13 Relation between velocity profile at $L_s=0.8\,d$ and L_m ($\psi=180°$)

extremely deformed flow at the section of $L_d=0.1\,d$ is restored gradually to the normal condition in course of flow along the pipe line. This time, the flow is considered to have a nearly uniform inward component of velocity. The model 1 in Fig. 10 shows this condition. The model 2 in the same figure shows the normal type of secondary flow due to bend. By combining the two flows, an abnormal flow picture 3 in Fig. 10 can be obtained. Figure 11 reveals equi-velocity regions at the section of $L_d=0.8\,d$, where the same results as by the others are also plotted. A remarkable displacement of a high velocity region can be seen. Closer examination of Fig. 9 shows that axially symmetric profile V_z is nearly re-established at the section $L_d=10\,d$ downstream from the elbow exit. Thus, when the second elbow is installed $10\,d$ downstream from the first elbow, the turned loss ζ will be considered to be independent of the twisted angle of pipe line.

4·2·2 Two dimensional double turn in the same plane ($\psi=0°$, $180°$)

In case of U turn, $\psi=0°$, the second elbow exaggerates the curved effects due to the first elbow. With a short spacer, $L_m=(0\sim0.65)\,d$, the axial velocity behind the second elbow is deformed much more than that due to a single elbow, the left of Fig. 12. Velocity profile of the axial component in N-plane is convexed and has an opposite form to that due to a single elbow. The same is true for the secondary flow component V_r in N-plane. This phenomenon is explained by use of the right side model in Fig. 10 B. Higher velocity range behind

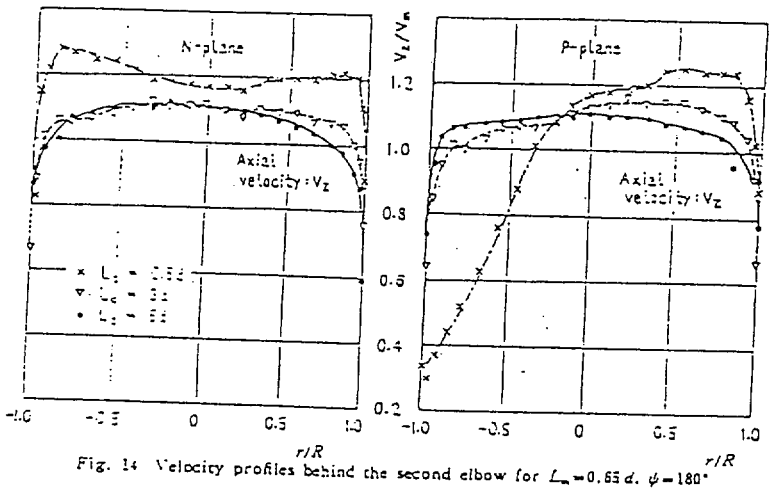

Fig. 14 Velocity profiles behind the second elbow for $L_m=0.65\,d$, $\psi=180°$

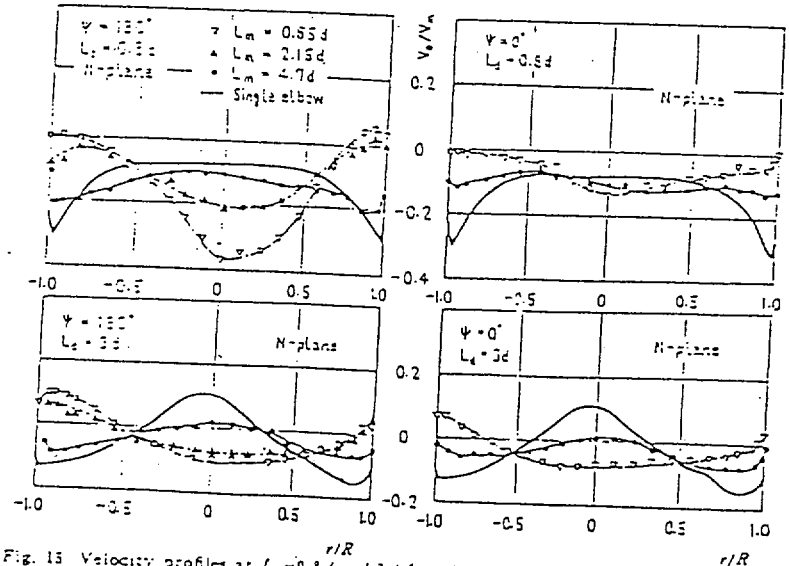

Fig. 15 Velocity profiles at $L_d=0.8\,d$ and $3\,d$ for pipes with a single elbow and two elbows

the first elbow dominates the greater parts of the outside of curvature as shown in the left of Fig. 20. On entering the second elbow with this velocity, a centrifugal force due to the fluid in the sections b-b and c-c exceeds that due to the fluid in the middle section a-a. In consequence, a secondary flow is set up in which the fluid near the section a-a moves inwards, the direction of which is opposite to that due to a single elbow. By increasing the spacer length, ($L_m=4.7\,d$ and $9.8\,d$), deformation of velocity distribution is greatly reduced before the second elbow and the secondary flow behind the elbow is nearly the same as the flow due to a single elbow.

In the flow in U turn, $\psi=0°$, a separation due to bends is much reduced as is seen in the velocity profile of Fig. 12. The above result verifies the fact in section 4-1, that the loss coefficient ζ for $\psi=0°$ diminishes with L_m. Figure 13 shows the velocity profile for S turn in the same plane. Profile of V_z in P-plane at the section of $L_s=0.8\,d$, just behind the elbow, is much deformed, but this profile is rapidly uniformalized along downstream from the second elbow, Fig. 14. By decreasing the spacer length L_m to $2.15\,d$ or less, the secondary flow having opposite sense to that observed behind a single elbow is observed in N-plane as shown in

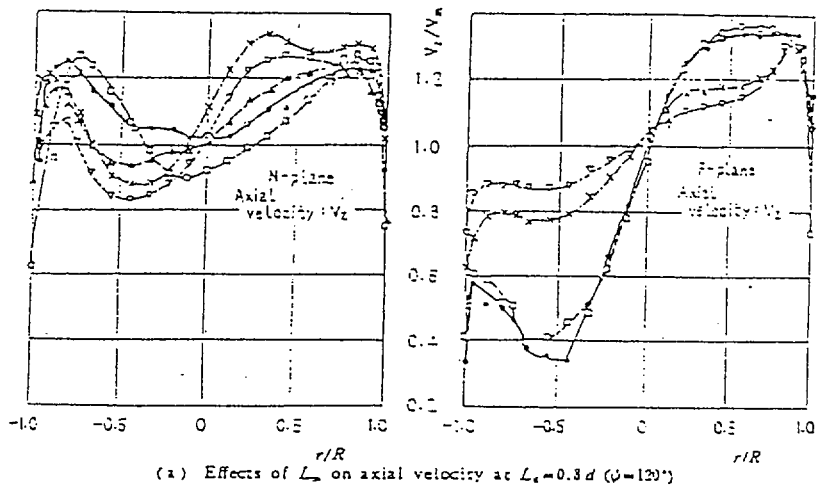

(a) Effects of L_m on axial velocity at $L_s=0.8\,d$ ($\psi=120°$)

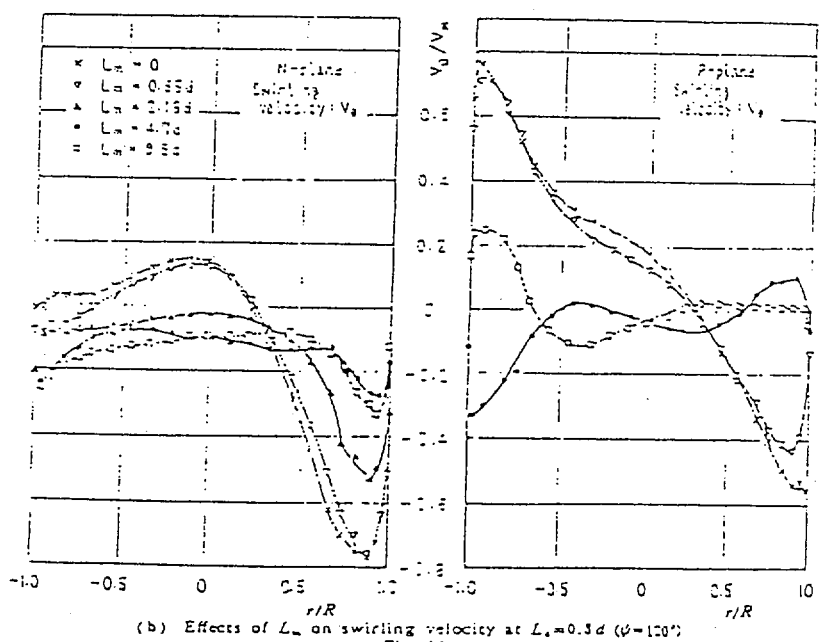

(b) Effects of L_m on swirling velocity at $L_s=0.8\,d$ ($\psi=120°$)

Fig. 16

fig. 10 B. Absolute value of this velocity V_s decreases as L_m is increased. When L_m is increased to 1.7 d or 9.8 d, the same direction of the secondary flow is observed as is in a single elbow, and the absolute value of V_s increases with L_m. From the above result an interesting conclusion may be deduced. Namely, for both cases, $\psi=0°$ and 180°, the sense of secondary flow V_s just behind the second elbow is reversed when the spacer length ranges $2.55<L_m/d<4.7$. When the spacer length L_m is less than this limit, a secondary flow occurs in the opposite direction to that due to the single elbow, and when L_m is longer the flow direction is reversed. Several examples of the secondary flow for $\psi=0°$ and 180° are shown in Fig. 15. The absolute value of V_s is generally greater for $\psi=180°$ than for $\psi=0°$. Comparing the above result on velocities, Figs. 13~15, with the turned losses in Fig. 7, an important conclusion is deduced that the loss coefficient ζ is closely related with the absolute value of the secondary flow. Namely, when $\psi=180°$, the values of $\zeta=1.63$, 1.54, 1.34, and 1.38 correspond to the cases for the spacer length of $L=0$, 0.65 d, 4.7 d and 20 d respectively.

4·2·3 Three-dimensional double turns in different planes ($\psi=120°$)

Figure 16 gives a relationship between velocity profiles and the spacer length for $\psi=120°$, where has nearly the greatest value. When the spacer short, a very complicated flow is generated behind the elbows, due to a strong interference between two elbows. As an example, Fig. 17(a) shows an equi-velocity diagram at the section $L_s=0.8\,d$. Higher velocity regions exist on the lines O-A_1 and O-B_N, corresponding to the outside of curvature of the second elbow and inside of the first one. Flow patterns in Fig. 17(a) differ remarkably from those in Fig. 11. Velocity profiles V_s of the secondary flow at section $L_s=0.8\,d$ are shown in Fig. 17(b). Strong clockwise swirling motions are recognized on the diameters of A_2-B_2, A_1-B_1, and A_3-B_3. On the other hand, a pair of clockwise and counter-clockwise vortices, one on O-B_2 being strong and clockwise, and the other on O-A_2 weak and counter-clockwise, is generated on the line A_2-B_2. Position of the weak vortex roughly corresponds to region of lower velocity and that of the strong vortex to region of higher velocity.

The maximum value of the secondary flow velocity is seen to reach as high as 90 percent of the mean flow velocity. Validity of the results in Fig. 17(b) is carefully checked by measuring the velocity in many diametral directions. The flow picture of section $L_s=0.65\,d$ is nearly the same as that of section $L_s=0$, and decay of the secondary flow along the pipe line is shown for $L_m=0.65\,d$ in Fig. 18(a). A pair of vortices which have already existed at the upstream section $L_s=0.8\,d$ is reduced to a single vortex at section $L_s=3\,d$, a strong vortex absorbing a weak one. In this process, the axial velocity is uniformalized. Figs. 16 and 18. At section $L_s=6\,d$, the single vortex takes a nearly forced vortex form, which reduces to zero along the pipe line, maintaining the form. This vortex producing a strong loss extends as far as 160 d downstream from the second elbow. If this kind of vortex is generated in the suction pipe of a pump or a blower, the performance will considerably be changed. When L_m is longer than 10 d, this forced vortex is not generated, the reason being the same

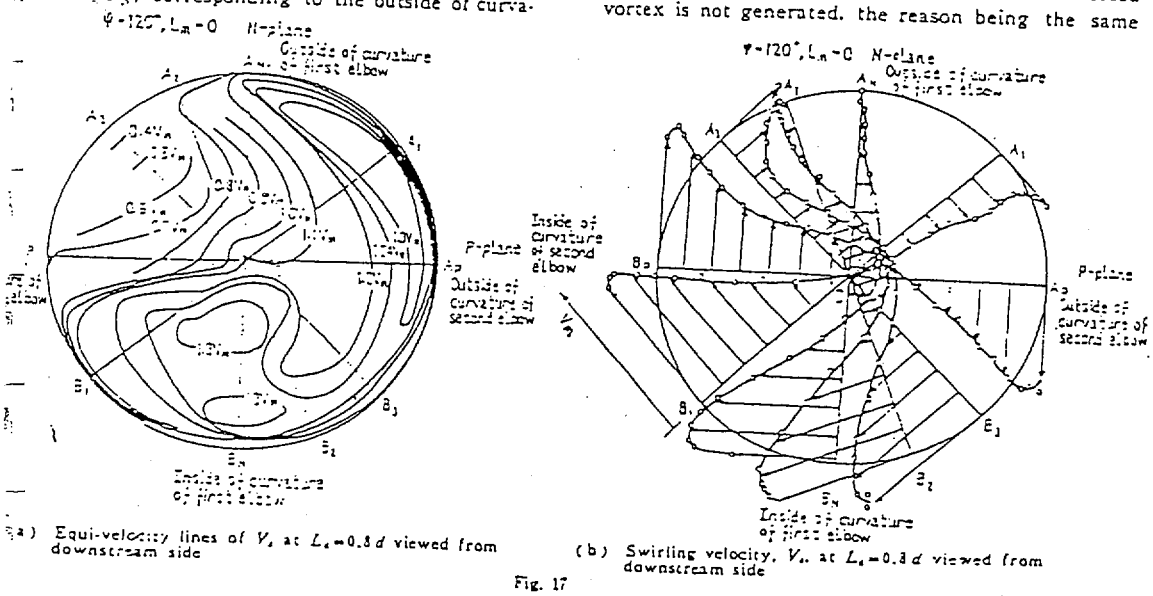

(a) Equi-velocity lines of V_s at $L_s=0.8\,d$ viewed from downstream side

(b) Swirling velocity, V_s, at $L_s=0.8\,d$ viewed from downstream side

Fig. 17

as given in section 4·2·2.

Figure 19 explains schematically the direction of vortex formation in a pipe downstream from the elbows. When water enters the second elbow with deformed flow conditions due to the first elbow, a centrifugal force acts in the second elbow as shown in the figure and a pair of strong and weak vortices is produced at the exit. The strong vortex absorbs the weak one and reduces to a single vortex, the sense coinciding to that of the strong vortex. Flow patterns for various bend conditions are shown diagrammatically in Fig. 20. The velocity profiles shown in pipe line correspond to the profiles on N-plane. The maximum velocity point is shown by a mark ×. Arrowed solid lines represent the direction and the magnitude of flow velocity on the pipe centre. Arrowed dotted lines and broken lines illustrate those near both sides of pipe wall. The velocity profiles above pipe line show those viewed from the downstream side.

5. Conclusions

A pipe line is turned in various configurations with two right-angled elbows and the following results

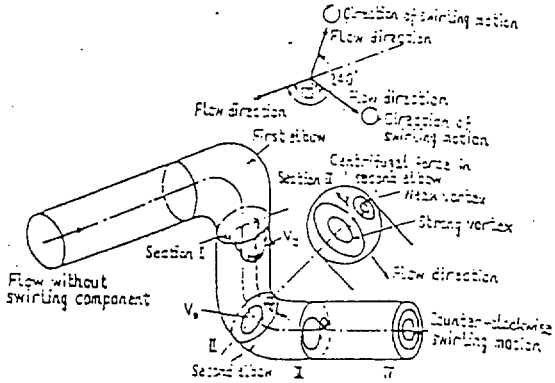

Fig. 19 Generation of swirling motion due to twisted pipe line

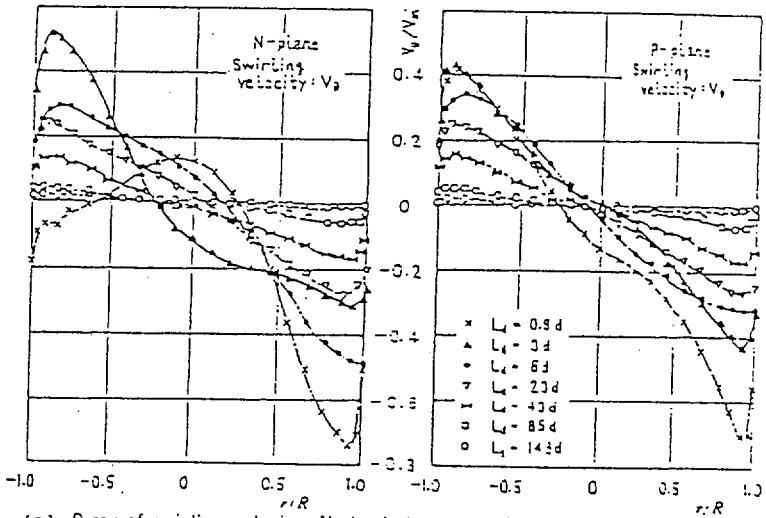

(a) Decay of swirling velocity, V_θ, behind the second elbow (L_m = 0.65 d, ψ = 120°)

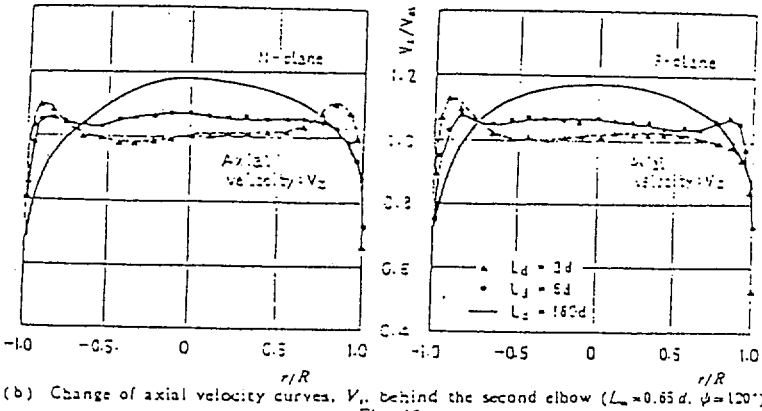

(b) Change of axial velocity curves, V_z, behind the second elbow (L_m = 0.65 d, ψ = 120°)

Fig. 18

are obtained:

(1) When the spacer length L_m is less than $5d$, the elbows interfer each other intensively and the turned loss becomes minimum for $\psi=0°$, maximum for $\psi=120°\sim150°$, and medium for $\psi=180°$. When $L_m \leqq 0.65d$, the loss exceeds twice that due to a single elbow, and when $L_m=10d$, the loss becomes independent of the twisted angle of pipe line.

(2) A secondary flow just behind a single elbow, $L_1=0.8d\sim3d$, shows an abnormal distribution, which recovers the normal condition at $L_1 \geqq 3$.

(3) With two elbows in the same plane, direction of a secondary flow behind the second elbow changes the sign when the spacer length L_m exceeds $2.15d\sim4.7d$.

(4) With two elbows in different planes, a forced type vortex is produced behind the bends when $L_m \leqq 4.7d$. The vortex becomes maximum at an angle $\psi=135°$ and it reaches about $135d$ downstream from the exit of the second elbow.

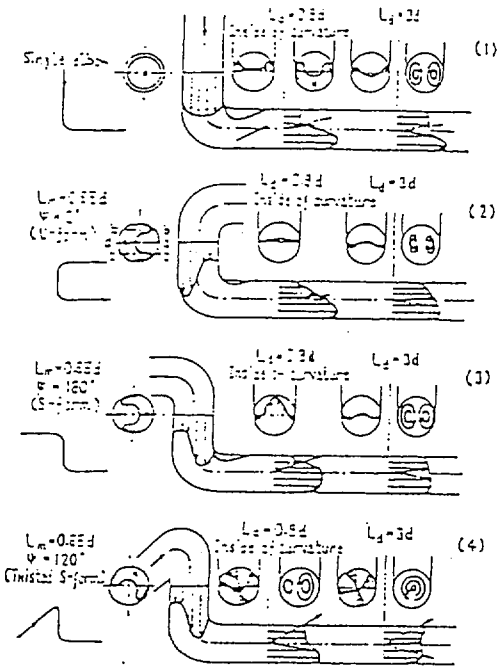

Fig. 20 Flow patterns for turned pipe line

References

(1) W.R. Dean: *Phil. Mag.*, Vol. 4 (1927), p. 208.
(2) M. Adler: *Z. AMM*, Vol. 14 (1934), p. 257.
(3) R.W. Detra: *Mitt. E.T.H.*, No. 20 (1953), p. 1.
(4) H. Ito: *Trans. ASME*, Ser. D, Vol. 82, No. 1 (1960-3), p. 131.
(5) A.V. Saph and E.V. Schoder: *Trans. A.S.C.E.*, Vol. 47 (1902), p. 1.
(6) J. Eustice: *Proc. Roy. Soc. Lond.*, Ser. A, Vol. 85 (1911), p. 119.
(7) C.I. Corp and H.T. Hartwell: *Bull. Univ. Wisconsin*, No. 66 (1927), p. 1.
(8) C.M. White: *Proc. Roy. Soc. Lond.*, Ser. A, Vol. 123 (1929), p. 645.
(9) H. Nippert: *Forsch. Geb. Ing.-Wesen*, 320 (1929), S. 1.
(10) J.R. Henry: *NACA ARR*, L4F 25.
(11) Ito and Imai: Preprint of *Japan Soc. Mech. Engrs.*, No. 153, (1966-4), P. 81, (in Japanese).

MPR

MPR Associates, Inc.
320 King Street
Alexandria, VA 22314

CALCULATION TITLE PAGE

Client Caldon, Inc.	Page 1 of 5
Project Point Beach LEFM Uncertainty Analysis	Task No. 157-076
Title Effect of LEFM Chordal Path Orientation on Measured Profile Factor	Calculation No. 157-076-SKK-02

Preparer/Date	Checker/Date	Reviewer/Date	Rev. No.
SON KIM 5/16/95	Matthew E. Roberts 5/16/95	DE Mazzola 5/16/95	0

MPR

MPR Associates, Inc.
320 King Street
Alexandria, VA 22314

RECORD OF REVISIONS

Calculation No.	Prepared By	Checked By	
157-076-SKK-02			Page 2

Revision	Description
0	Original Issue

TABLE OF CONTENTS

1.0 PURPOSE

Flow tests were performed at Alden Research Laboratory in which a four-path chordal leading edge flow meter (LEFM) was installed in two different piping configurations. [

]

2.0 SUMMARY

[

]

3.0 DISCUSSION

[

]

The data from these two tests were entered into a Microsoft Excel 5.0 worksheet, and average profile factors were calculated for each piping configuration and LEFM orientation, using the following expression for profile factor:

$$PF = \frac{Q_{arl}}{Q_{lefm}}$$

where:

Q_{LEFM} = volumetric flow rate calculated by LEFM from V_{axial}

Q_{ARL} = actual volumetric flow rate based on ARL weigh tank

A printout of the Excel worksheet is provided in Attachment 1. The results are summarized in Section 2.0.

4.0 REFERENCES

1. Alden Research Laboratory Report No. 82-95/C730, "Calibration of Two 16" Leading Edge Flow Meters, Caldon, Inc., Prairie Island Nuclear Plant Model," April 1995.

2. "Results of February and July 1978 LEFM Hydraulic Tests at Alden Labs" OEM 78-40, Westinghouse Electric Corporation, Oceanic Division, 2/7/79.

MPR

MPR Associates, Inc.
320 King Street
Alexandria, VA 22314

CALCULATION TITLE PAGE

Client Caldon, Inc.	Page 1 of 12
Project Point Beach LEFM Uncertainty Analysis	Task No. 157-076
Title Hydraulic Profile and Its Uncertainty - Unit 2	Calculation No. 157-076-JAR-1

Preparer/Date	Checker/Date	Reviewer/Date	Rev. No.
Jennifer Ryan 5/16/95	Matthew E. Roberts Matthew E. Roberts 5/16/95	D. E. Mazzola D. E. Mazzola 5/16/95	0

MPR

MPR Associates, Inc.
320 King Street
Alexandria, VA 22314

RECORD OF REVISIONS

Calculation No.	Prepared By	Checked By	Page 2
157-076-JAR-1	J. Reyes	M. Roberts	

Revision	Description
0	Original Issue

TABLE OF CONTENTS

1.0 PURPOSE

The Leading Edge Flow Meter (LEFM) calculates volumetric flow from fluid velocity measurements along acoustic paths in a measurement section or spool piece. The relationship between the velocity measured along the acoustic paths and the volumetric flow is determined by (a) the angle between the acoustic paths and the axial fluid velocity vectors which intersect them and (b) a profile factor which relates the axial velocities along the acoustic paths to the axial velocity averaged over the cross section of the spool piece. This calculation provides the basis for the profile factor to be used with the four-path chordal flow meter installed at Point Beach Unit 2, and calculates the uncertainty bounds on the profile factor.

2.0 SUMMARY

A profile factor of [ ] should be used with the four-path chordal flow meter at Point Beach Unit 2, and the uncertainty in this profile factor is [ ].

3.0 APPROACH

The profile factor and its accuracy for a four-path chordal flow meter are dependent upon the ability of the meter to integrate from discrete velocities measured on each of four paths into the spatially averaged velocity across the spool piece section. This integration is affected by the inaccuracy of the four path Gaussian Quadrature integration method, and the fact that the velocity profile is not uniform across the section. The velocity profile is non-uniform on two counts. First, in long straight sections of pipe the velocity profile becomes rounded, blunt and symmetrical, characterized as "fully developed". In a fully developed profile, the velocity has a maximum at the fluid center and minimum at the pipe wall. Secondly, actual piping systems like the Point Beach feedwater system contain bends and other fittings which produce, in varying degrees, asymmetrical distortions that change the velocity gradients and introduce secondary non-axial flows.

To estimate the Point Beach Unit 2 four-path chordal profile factor and its uncertainty, this calculation takes the following approach:

(1) [

]

(2) [

]

(3) [

]

4.0 CALCULATION

4.1 Profile Factor and Uncertainty for Fully Developed Turbulent Flow

Reference 1 establishes a profile factor versus Reynolds' Number for measurement of fully developed flow using a four-path chordal flow meter. The reference analyzes calibration data taken at Alden Research Laboratories on eight Westinghouse LEFM spool pieces in the 1979 through 1983 time frame. A mean profile factor of 1.0012 is calculated in the Reynolds' Number range of 3×10^6 for over 160 weigh tank runs. This result is extrapolated to the 3×10^7 Reynolds' Number range existing in feedwater piping using two empirical correlations for velocity profiles of fully developed turbulent flow. The resulting profile factor for fully developed flow is 1.0010 with an uncertainty of ± 0.20% assuming a 95% level of confidence (Reference 1 defines the profile factor as 0.9950, which is equal to 1.0010 multiplied by 0.994, the Gaussian Quadrature integration error for a circular cross-section).

4.2 Point Beach Unit 2 Hydraulic Geometry Effects

The piping arrangement and flow meter orientation in the Point Beach Unit 2 feedwater piping are sketched in Figure 1 (Reference 2). The flowmeter is located in a straight run of horizontal piping approximately 47 pipe diameters downstream of an elbow. In turn, the elbow is approximately 3 diameters downstream of a converging tee. One of the lines feeding this tee is perpendicular to the plane of the elbow. A converging tee is located in the straight run of horizontal piping 31 pipe diameters upstream of the LEFM. However, the line feeding this tee is a bypass line which is normally closed; no additional hydraulic effect is anticipated.

[

]

[

]

Murakami has extensively tested non-coplanar bends. Murakami's data (attached to this calculation) shows that a swirl, once created, may persist for up to 150 pipe diameters. On the basis of Murakami's data, the swirl should be detectable at the LEFM location 47 diameters from the elbow. Evaluation of the LEFM in-situ path velocity data confirms the presence of a swirl in the expected direction.

Figure 1 shows the orientation and numbering of the LEFM paths at Point Beach Unit 2. Individual path velocities recorded during commissioning of the LEFM at Point Beach Unit 2 are summarized in Table 1 below, for which the following nomenclature applies:

[

]

[

]

[

]

[

]

4.3 Velocity Profile Asymmetry Effects

All four of the LEFM acoustic paths measure the fluid velocity in the same spatial plane. Accordingly, asymmetries in the velocity profile have the potential to cause measurement error. In the case of Point Beach Unit 2, the potential sources of asymmetry in the velocity profile are:

- Axial velocity profile asymmetry due for example to the upstream bend, misalignment of the LEFM spoolpiece with the upstream pipe, or variations in pipe roughness.
- [

]

[

]

4.4 Combination of Errors

- [ ]
- [ ]

- [ ]
- [ ]
- [ ]

[ ]

5.0 REFERENCES

1. MPR Calculation Number 15708HE1A, "Determination of the Profile Factor and Its Uncertainty for a 4 Path LEFM in Long Straight Pipe," Rev. 0, H. Estrada, 12/18/82.

2. Bechtel Drawing No. P-222, Rev. 3 (Job No. 10447), "Main Feed Water From 2HX21A and B to 16" EB-9 (DB-1), Unit 2."

3. Murakami, M., Shimizu, Y., and Shiragumi, H., "Studies on Fluid Flow in Three Dimensional Bend Conduits," Japan Society of Mechanical Engineers (JSME) Bulletin V. 12, No. 54, Dec. 1969, pp 1369-1379.

4. Caldon Procedure No. EFP56, "Installation and Commissioning of LEFM 8300," Completed 3/9/95 for Point Beach Unit 2 Installation by M. Brink (Caldon) and E. Miller (MPR).

5. MPR Calculation Number 108-054-LAS-03, Rev.0, "Average Chordal Velocities for Universal Fluid Velocity Model."

6. Abernathy et al, "ASME Measurement Uncertainty," ASME Journal of Fluids Engineering, Vol. 107, p. 161-164, June 1985.

7. MPR Calculation No. 157-076-SKK-02, Rev. 0, "Effect of LEFM Chordal Path Orientation on Measured Profile Factor."

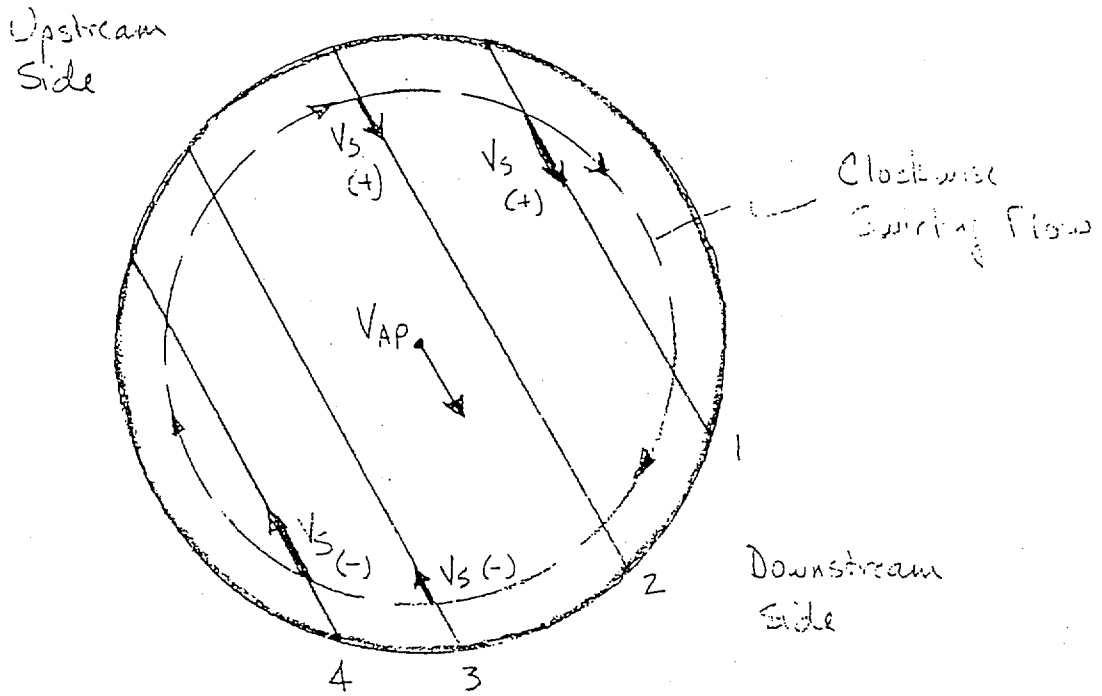

V_{AP} = Direction of Axial Flow Projected on All paths

FIGURE 2

Effect of Axisymmetric Swirl on LEFM Path Velocities

Attachment 1

Japan Society of Mechanical Engineers (JSME), Bulletin, vol. 12, no. 54, Dec. 1969, pp. 1369-1379.

532.542 : 532.55

Studies on Fluid Flow in Three-Dimensional Bend Conduits*

By Mitsukiyo MURAKAMI**, Yukimaru SHIMIZU***, and Heiji SHIRAGAMI****

This paper gives the results of the experimental study of loss and secondary circulation due to various combinations of commercial elbows, and discussed the relationship between the loss and the circulation. Three general combinations are: One where the two elbows produce a complete reversal in the direction of flow, termed the "U" bend; and two where the two elbows produce an offset but no change in direction, termed the "S" bend; and three where the two elbows produce both an offset and a 90 degree change in the direction of flow, termed the "twisted S" bend.

The last combination gives rise to a strong single spiral motion in the straight pipe of curved pipes downstream and shows the maximum bend loss.

1. Introduction

A pipe line of a fluid machine or other hy-ulic plants has often many complicated curved tions. When a fluid flows through such a curv-ipe, the fluid acquires a secondary flow com-t, which would not present itself in a straight flow. The secondary flow produces an addition-hydraulic loss. Particularly when two curved s are located in different planes, a strong spiral ion is produced in the pipe and the distribution he exit velocity is deformed remarkably, result-in a great loss. When the fluid enters a fluid hine or a flow meter with the deformed veloc-it alters their performances considerably.

Many studies[(1)-(11)] on this subject have been e in the past, but the most of them concern the hydraulic loss on smooth bends having a tively larger radius of curvature. A right-angled mercial elbow has a relatively small bend s and also a sudden contraction or enlargement e sections of screw joints, which complicates flow patterns and prohibits a theoretical ap-h.

The object of this paper is to clarify experi-ally the relationship between hydraulic loss and ity distribution of two elbows located succes-y in a pipe line.

Received 27 th July, 1968.

Professor, Faculty of Engineering, Nagoya University.
Assistant, Faculty of Engineering, Nagoya University, Chikusa-ku, Nagoya.
Engineer, Mitsubishi Heavy Industry Co.

2. Nomenclature

d: diameter of pipe
g: acceleration of gravity
H: total loss of head in gauge length
L_d: distance of downstream pressure tap (section 9 in Fig. 2) from exit of the second elbow
L_m: length of spacer between the first and the second elbows
L_u: distance of upstream pressure tap (section 0 in Fig. 2) from entrance of the first elbow
L: $L_d+L_m+L_u$, total gauge length
r: radial distance
R: radius of pipe
p_1: static pressure at section 0 in Fig. 2
p_2: static pressure at section 9 in Fig. 2
p_s: wall pressure at any section downstream from the second elbow
V_z: axial component of velocity
$V_{z\max}$: maximum value of V_z
V_θ: tangential component of velocity
$V_{\theta\max}$: maximum value of V_θ
V_m: mean velocity calculated from orifice readings
γ: specific weight of water
ρ: radius of curvature of curved pipe
ζ: coefficient of total loss due to two elbows as defined by Eq. (1)
ζ_t: coefficient of apparent total loss due to two elbows, calculated by Eq. (1) with p_1 and p_2
ζ_0: coefficient of loss due to a single elbow in a pipe line

λ: friction factor for straight pipe

ψ: angle of pipe line twisted by two elbows, as defined by Fig. 3

Notations in Fig. 3

N-plane: plane normal to bend surface of the second elbow

P-plane: bend plane of the second elbow

Suffix

N: normal direction to P and Z and on N-plane

P: normal direction to N and Z and on P-plane

Z: downstream direction along pipe line.

3. Experimental apparatus and procedure

The general arrangement of the test apparatus is indicated in a schematic diagram, Fig. 1. A steady pressure was maintained in the metering system by a head tank for low-pressure range and by a centrifugal pump for high-pressure range. A flexible pipe was employed to facilitate the bend configuration of pipe line. The flow rate of the piping system was measured by an orifice meter. The measuring pipes 6, 8, and 10 are of brass and the inside diameters are 53.75, 53.84, and 53.90 mm respectively, and the pipes have hydraulically smooth surface. The details of measuring pipes are shown in Fig. 2. Distance of two elbows, namely, the spacer length and an angle of twist of pipe line used in this experiment are given in Table 1. Each measuring section has four taps, the diameter of which is 1 mm and equally spaced circumferentially. The upstream section 0 is located 35 pipe diameters downstream from the rectifying tank to eliminate the effects of the inlet length*. The measuring section 9 downstream from the second elbow is selected at the position where the effect of elbows disappears. Depending on the twisted angle ψ and the length of spacer L_m, the position of the section changes from 150 to 300 diameters downstream from the second elbow. The position was selected on the basis of pressure distribution along the pipe line and velocity profiles of the pipe sections.

To avoid an error due to fluctuation of manometer readings, a rotary cock is inserted in all the pressure transmitting pipes from taps to manometers. After closing the cock, the manometer readings were taken. A cylindrical pitot tube with three holes was traversed in the sections shown by dotted lines a~h in Fig. 2 and velocity profile was obtained (tube diameter=3.025 mm, hole diameter=0.3 mm). To check the accuracy of measurements, the flow quantity evaluated by a graphical integration of axial component of velocity was compared with that by the orifice meter. The difference was proved to be less than 5 percent.

Coefficient of the total fitting loss due to two elbows located in series in a pipe line is calculated by the following equation:

$$H=\frac{p_1-p_2}{\gamma}=\lambda\left(\frac{L}{d}\right)\left(\frac{V_m^2}{2g}\right)+\zeta\left(\frac{V_m^2}{2g}\right)\cdots\cdots\cdots\cdots(1)$$

Table 1 Length of spacer L_m/d and angle of turn ψ of pipe line employed in this test

L_m/d	0	0.65	2.15	4.7	9.8		
ψ	0°	45°	90°	120°	135°	140°	180°

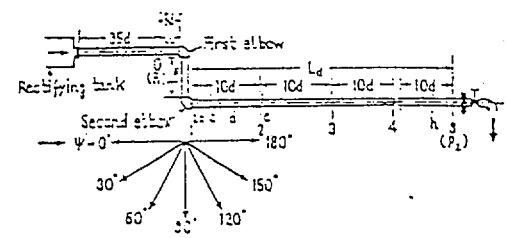

1~9 : Measuring sections of pressure
a~h : Measuring sections of velocity
a : 0.1 d from the second elbow
b : 0.5 d
c : 3 d
:
:
h : (150 250) d

Fig. 2 Measuring sections and angle of turn of pipe line

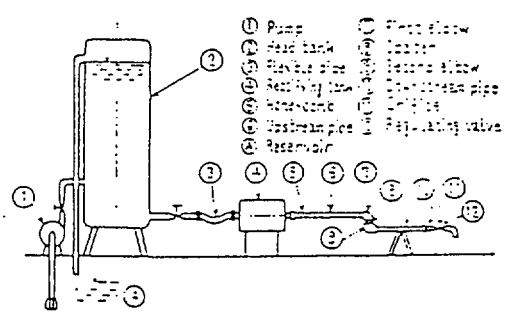

Fig. 1 Schematic diagram of test arrangement

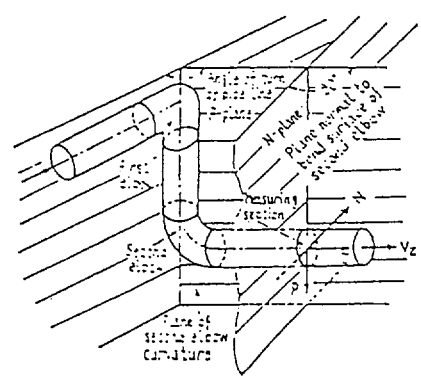

Fig. 3 Definition of sections and directions

* The effects of the inlet length on ζ are negligible when the length ranges from 5 to 35 pipe diameters.

hen a single elbow is in a pipe line, the loss coef-ent ζ in Eq. (1) reduces to ζ_0, the loss coefficient to a single elbow.

4. Experimental results and discussion

4·1 Loss of head by two 90-degree elbows

Hydraulic losses due to combination of two lbows have been studied by many investigators. But knowledges of the distortion of velocity at the bend exits and its relations with the hydraulic loss re not sufficient. In the following, results of this xperiment on head loss due to bends are summariz-d and compared with those obtained by the other nvestigators.

4·1·1 Pipe length required to recover normal stribution of velocity

Due to generation of a secondary flow by pipe ends, distributions of velocity and pressure in a pe section downstream from the bends are distort-considerably. The secondary flow decays toward ownstream and the distortion of the velocity is adually recovered to the normal flow conditions. us, by examining the pressure drop along the e downstream from the second elbow, position of e nearest section at which the normal flow con-tions will be re-established can be found.

In Fig. 4 apparent coefficient of loss ζ_t by Eq.) is plotted against L_d/d, where the wall pres-p_t downstream from the second elbow is used in place of p_1. As the measuring section of p_t is kept away from the second elbow, ζ_t tends to a constant value, i.e. the true fitting loss of the bend ζ. Apparently, by introducing a short length of a pipe L_m, namely a spacer, between the two elbows, the value of bend loss ζ is altered. For reference, results of a single elbow in a pipe line are also plotted. In this case, ζ reaches a constant value of 0.735, the true loss coefficient, when the wall pressure p_t at section of $L_d=50\,d$ is used. When two elbows are located in U ($\psi=0°$) and S ($\psi=180°$) forms in the same plane, ζ_t flattens off in a shorter length. When two elbows are off set in the twisted S form, for example $\psi=120°$ and 140°, the turned effects extend as far as $L_d=160\,d$. The above results show that the required pipe length in which the turned effect disappears from the pipe line will be much altered by the turned form. Table 2 gives this required pipe length, which is unaffected by Reynolds number in this experimental range.

. 2 Minimum pipe length L_d behind the second elbow to recover normal flow conditions

L_m/d \ ψ	0°	45°	90°	135°	180°
0	($\psi=5°$) * 45	100	180	180	45
0.65	($\psi=2.5°$) 45 *	110	160	160	80
4.7	50	60	80	80	80

* For very short spacer length L_m/d of 0 and 0.65, pipe line can not be turned strictly U-shape.

4·1·2 Coupling depth of screw joint and hydraulic loss

The coupling depth of a screw joint between an elbow and a pipe has a considerable effect on the fitting losses of the elbow. Figure 5 shows the results of experiments, where the two elbows are located in S form in the same plane. Depending upon the coupling condition of screw joints the fitting loss is seen to be scattered about 15 percent. Throughout this paper, with exception of the present section, the loss of elbows is referred to the case when the pipe ends are fully screwed to the coupling parts.

4·1·3 Effects of twisted angle ψ and spacer length L_m between two elbows on turned loss

Figure 6 shows the relation between ζ and ψ for various values of L_m/d. With small value of L_m/d, ζ is much affected by ψ. From a minimum value of $\psi=0°$, ζ increases and takes a maximum

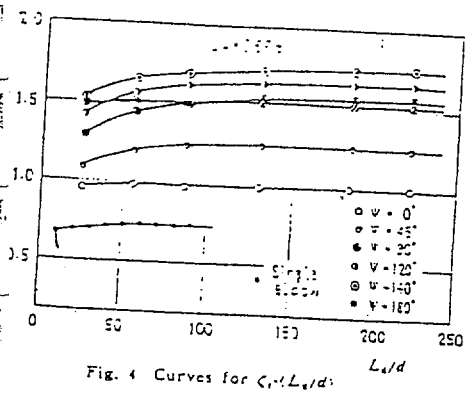

Fig. 4 Curves for ζ_t-(L_d/d)

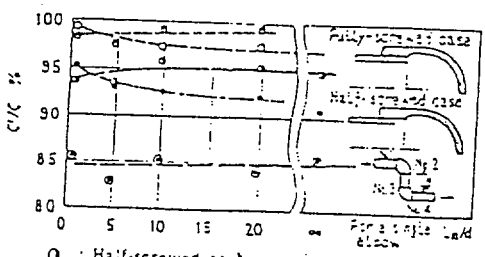

O : Half-screwed at No. 1 only
◐ : Half-screwed at No. 2 only
○ : Half-screwed at No. 3 only
● : Half-screwed at No. 4 only
◐ : Half-screwed at all joints
ζ' = Loss coefficient in Half-screwed case
ζ = Loss coefficient in Fully-screwed case

Fig. 5 Relation between screwed depth of joints and loss coefficients

value at about $\psi=130°\sim140°$, and again it decreases to the value of $\psi=180°$. For reference, twice the loss of a single elbow, $2\zeta_0$, is shown in Fig. 6. When length of the spacer L_m is less than $4.7\,d$, ζ has a maximum and it exceeds the value $2\zeta_0$ at an angle $\psi\fallingdotseq80°$. When $L_m=4.7\,d$, the maximum value becomes less than $2\zeta_0$ and is changed by the twisted angle ψ of pipe line. When $L_m\geqq10\,d$, ζ is independent of the angle ψ and remains constant. The value, however, is appreciably less than twice the single elbow loss, $2\zeta_0$, exhibiting an existence of interference of elbows. Even with this interference, loss of the combined elbows is independent of the twisted angle. The reason is clarified by examining the velocity profile downstream from the first elbow. The velocity is seen to be distributed nearly in axial symmetry but is not fully developed, the details of which will be described later.

In the past, several investigators[7][10][11] have measured the turned loss of two bends combined and they all observed an existence of a maximum loss at about an angle $\psi=90°$, and the value was always less than twice the single elbow loss, $2\zeta_0$, the results being different from the above. The reason will probably be attributable to the fact that the past experiments were made with smooth curved pipes having a larger radius of curvature ($\rho/d\geqq2$).

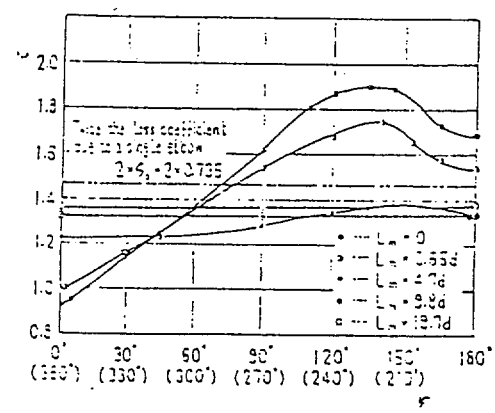

Fig. 6 $\zeta-\psi$

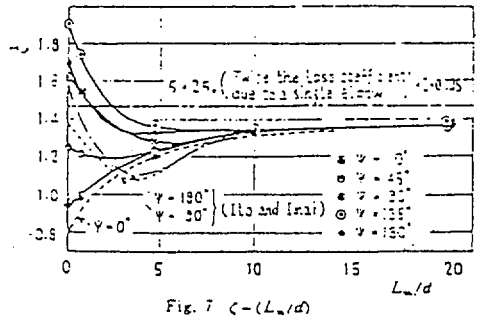

Fig. 7 $\zeta-(L_m/d)$

Relation between ζ and L_m/d is plotted for several values of ψ in Fig. 7, where Ito's data[11] are also given. ζ changes sharply within the small range of $L_m/d<5$. When ψ is less than 45°, ζ increases with L_m, but when $\psi\geqq45°$, ζ decreases to one minimum value and again increases as L_m is increased. In all cases, the loss mentioned the above are proved to be unaffected by Reynolds number in this experimental range and hence its descriptions are omitted. However, when the pipe line is bent three-dimensionally with an angle $\psi=90°\sim180°$, and the length of spacer L_m is reduced to zero, a few percentage variations of the turned loss is seen by change of Reynolds number.

4·2 Distribution of velocity

4·2·1 Single curved pipe (with one elbow)

Due to sudden enlargements or contractions in elbow joints, the flow pattern is much disturbed and

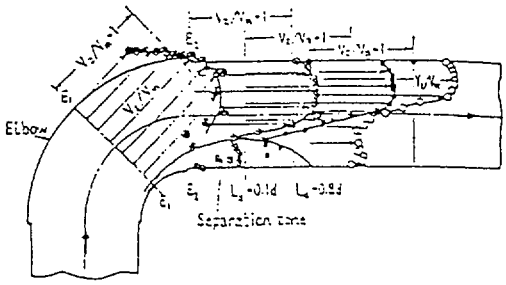

(a) Distribution of axial velocity in bend plane (N-plane), (Single elbow)

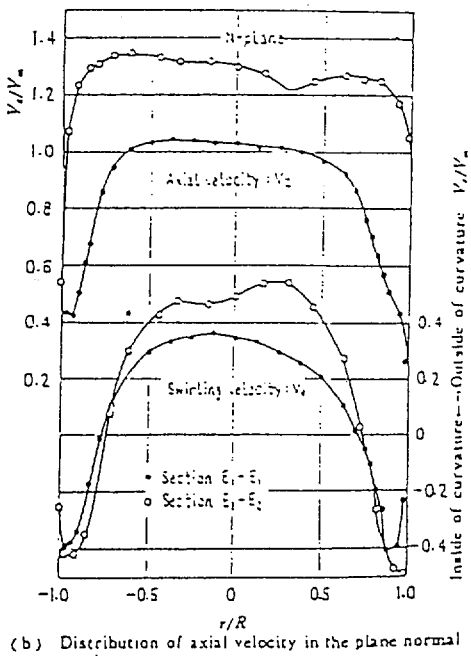

(b) Distribution of axial velocity in the plane normal to N-plane

Fig. 8

curate measurements of velocity distribution in the elbow will encounter great difficulty. Figure 8 (a) and (b) show velocity profiles in an elbow. At the middle section E_1-E_1 of the elbow, Fig. 8(a), higher velocity is observed inside the curvature, the flow resembling a free vortex motion. The axial velocity on N-plane, Fig. 8 (b), of the same section has nearly an even distribution. On the other hand, a fairly intensive secondary flow is set up in this section. As a result, the maximum axial velocity is further displaced from the centre of pipe towards the outer wall. Thus a considerable elevation of the axial velocity is seen near the outer wall. At the same time, the flow velocity near the centre is reduced gradually, resulting in a concave velocity profile. N-plane. In addition, sharp bend

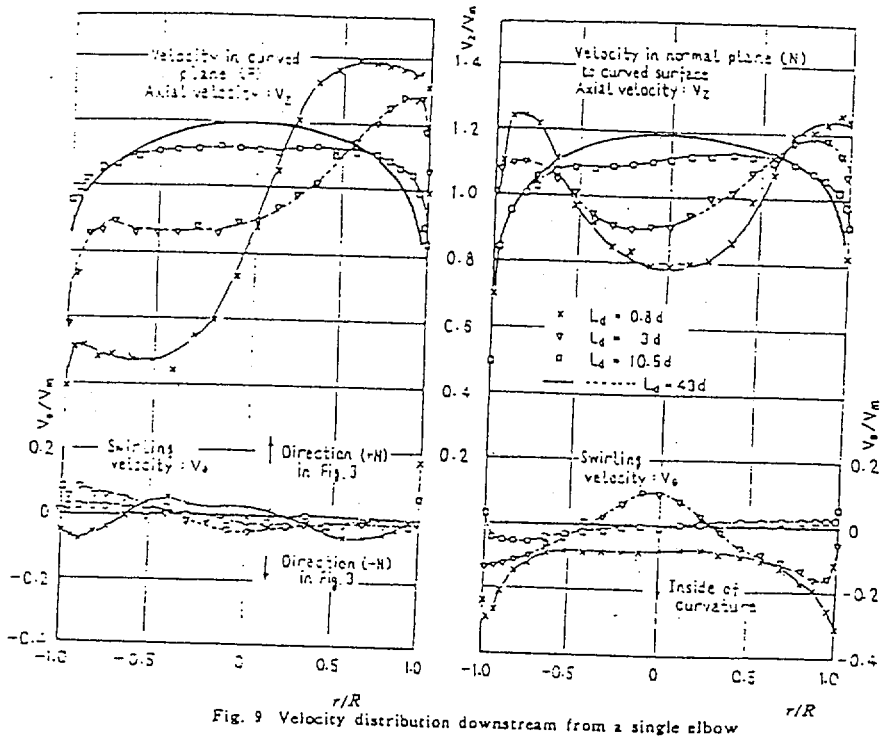

Fig. 9 Velocity distribution downstream from a single elbow

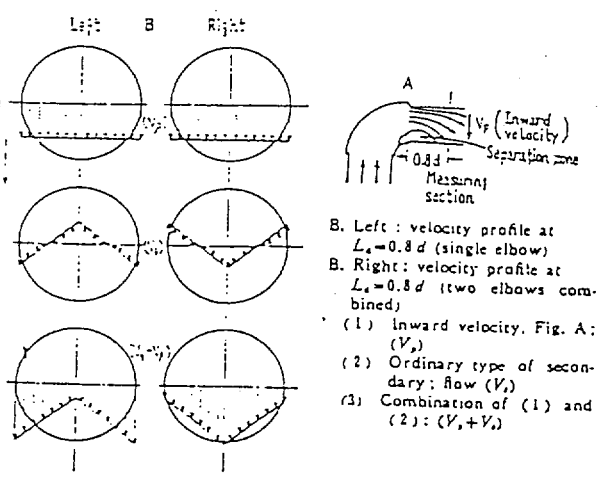

B. Left : velocity profile at $L_d = 0.8\,d$ (single elbow)
B. Right : velocity profile at $L_d = 0.8\,d$ (two elbows combined)
(1) Inward velocity, Fig. A: (V_F)
(2) Ordinary type of secondary flow (V_s)
(3) Combination of (1) and (2): ($V_F + V_s$)

10 Explanation of abnormal type of secondary flow behind elbows

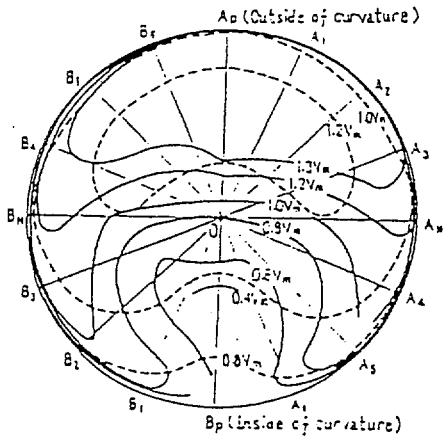

— Present Test, $\rho/d \fallingdotseq 1$, $R_e = 10^5$
— Adler, $\rho/d = 100$, $R_e = 1.17 \times 10^4$

Fig. 11 Equi-velocity lines at $L_d = 0.8d$, (V_s)

of the elbow develops a flow separation at the inner wall of the section E_1-E_1, which accentuates the uneven distribution of axial velocity. Thus, a maximum displacement of the axial velocity occurs near the section $L_d=0.1\,d$, just after the elbow exit, and after the section the velocity is recovered gradually to that of the normal flow condition, Fig. 9. An abnormal type of secondary flow is seen at section $L_d=0.8\,d$, where all of the fluids in N-plane move inwards of the curvature. The reason why this type flow occurs can be studied on a simple model as shown in the left of Fig. 10. The ex-

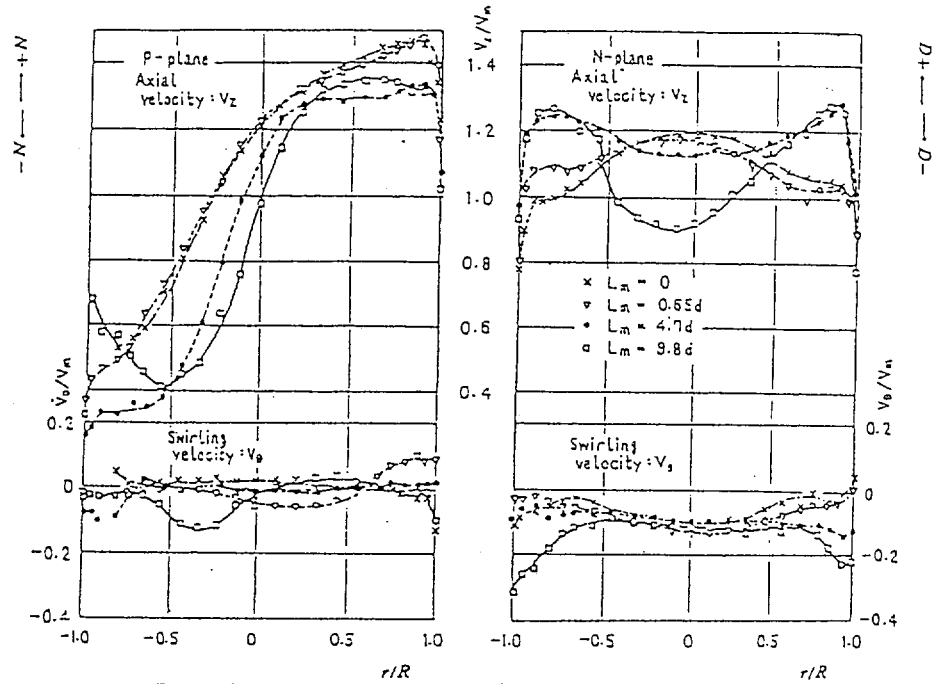

Fig. 12 Relation between velocity profile at $L_d=0.6\,d$ and L_m. ($\psi=0°$)

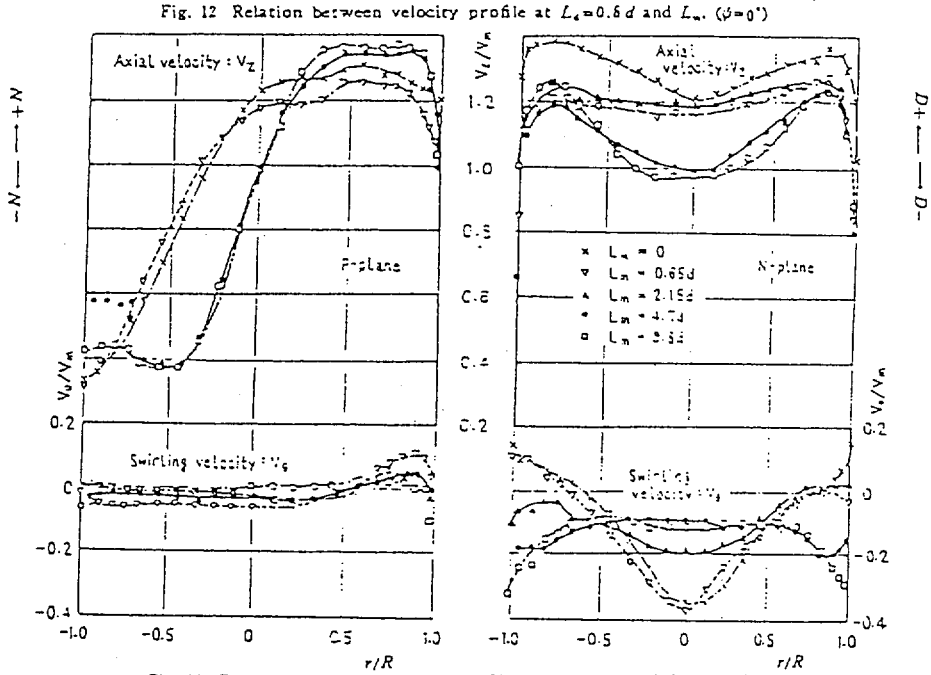

Fig. 13 Relation between velocity profile at $L_d=0.8\,d$ and L_m. ($\psi=180°$)

extremely deformed flow at the section of $L_d=0.1\,d$ is restored gradually to the normal condition in course of flow along the pipe line. This time, the flow is considered to have a nearly uniform inward component of velocity. The model 1 in Fig. 10 shows this condition. The model 2 in the same figure shows the normal type of secondary flow due to bend. By combining the two flows, an abnormal flow picture 3 in Fig. 10 can be obtained. Figure 11 reveals equi-velocity regions at the section of $L_d=0.8\,d$, where the same results as by the others[2] are also plotted. A remarkable displacement of a high velocity region can be seen. Closer examination of Fig. 9 shows that axially symmetric profile V_z is nearly re-established at the section $L_d=10\,d$ downstream from the elbow exit. Thus, when the second elbow is installed $10\,d$ downstream from the first elbow, the turned loss ζ will be considered to be independent of the twisted angle of pipe line.

4·2·2 Two dimensional double turn in the same plane ($\psi=0°$, $180°$)

In case of U turn, $\psi=0°$, the second elbow exaggerates the curved effects due to the first elbow. With a short spacer, $L_m=(0\sim0.65)\,d$, the axial velocity behind the second elbow is deformed much more than that due to a single elbow, the left of Fig. 12. Velocity profile of the axial component in N-plane is convexed and has an opposite form to that due to a single elbow. The same is true for the secondary flow component V_r in N-plane. This phenomenon is explained by use of the right side model in Fig. 10 B. Higher velocity range behind

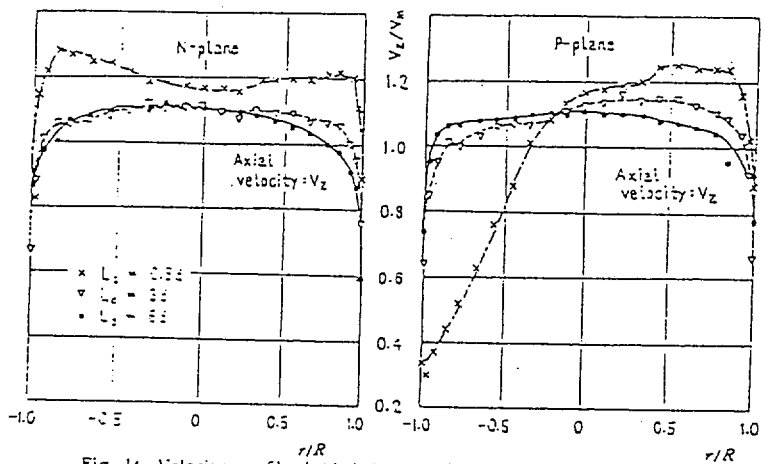

Fig. 14 Velocity profiles behind the second elbow for $L_m=0.65\,d$, $\psi=180°$

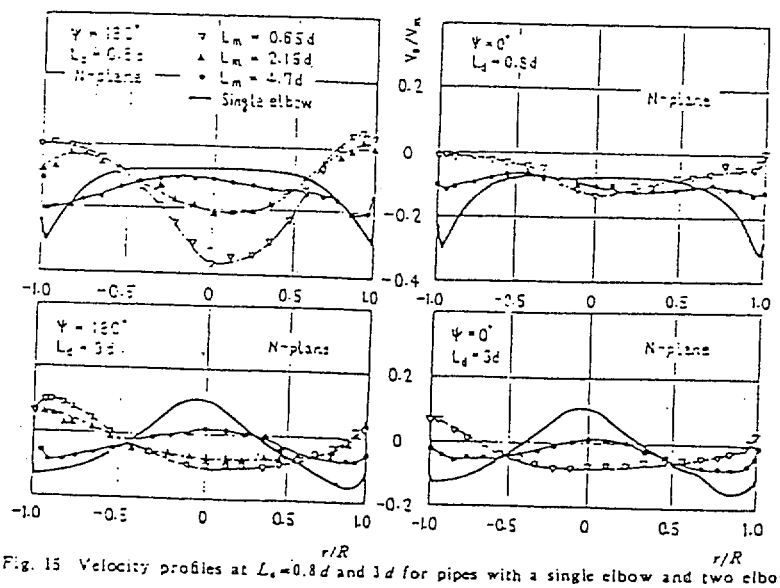

Fig. 15 Velocity profiles at $L_d=0.8\,d$ and $3\,d$ for pipes with a single elbow and two elbows

the first elbow dominates the greater parts of the outside of curvature as shown in the left of Fig. 20. On entering the second elbow with this velocity, a centrifugal force due to the fluid in the sections b-b and c-c exceeds that due to the fluid in the middle section a-a. In consequence, a secondary flow is set up in which the fluid near the section a-a moves inwards, the direction of which is opposite to that due to a single elbow. By increasing the spacer length, ($L_m=4.7\,d$ and $9.8\,d$), deformation of velocity distribution is greatly reduced before the second elbow and the secondary flow behind the elbow is nearly the same as the flow due to a single elbow.

In the flow in U turn, $\psi=0°$, a separation due to bends is much reduced as is seen in the velocity profile of Fig. 12. The above result verifies the fact in section 4·1, that the loss coefficient ζ for $\psi=0°$ diminishes with L_m. Figure 13 shows the velocity profile for S turn in the same plane. Profile of V_z in P-plane at the section of $L_e=0.8\,d$, just behind the elbow, is much deformed, but this profile is rapidly uniformalized along downstream from the second elbow, Fig. 14. By decreasing the spacer length L_m to $2.15\,d$ or less, the secondary flow having opposite sense to that observed behind a single elbow is observed in N-plane as shown in

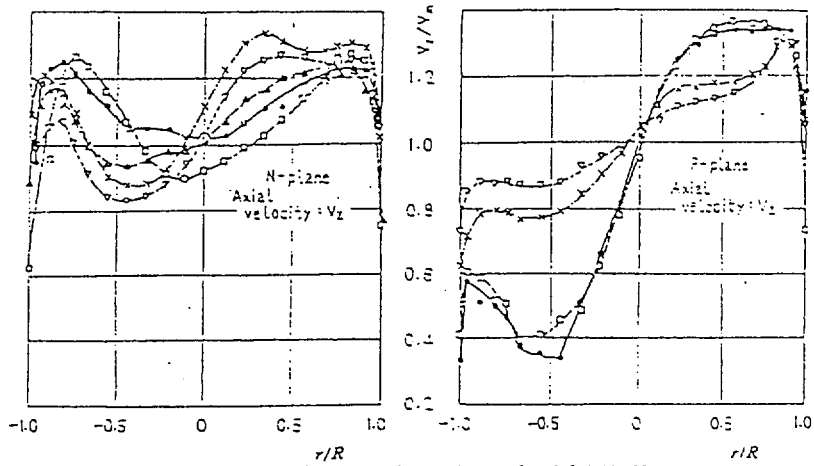

(a) Effects of L_m on axial velocity at $L_e=0.8\,d$ ($\psi=120°$)

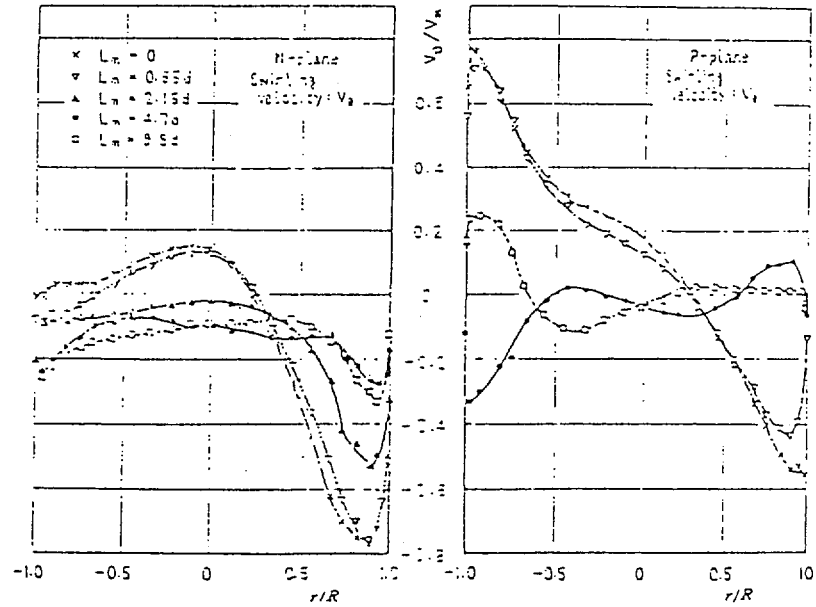

(b) Effects of L_m on swirling velocity at $L_e=0.8\,d$ ($\psi=120°$)

Fig. 16

Fig. 10 B. Absolute value of this velocity V_s decreases as L_m is increased. When L_m is increased to 1.7 d or 9.8 d, the same direction of the secondary flow is observed as is in a single elbow, and the absolute value of V_s increases with L_m. From the above result an interesting conclusion may be deduced. Namely, for both cases, $\psi=0°$ and 180°, the sense of secondary flow V_s just behind the second elbow is reversed when the spacer length ranges $2.55<L_m/d<4.7$. When the spacer length L_m is less than this limit, a secondary flow occurs in the opposite direction to that due to the single elbow, and when L_m is longer the flow direction is reversed. Several examples of the secondary flow for $\psi=0°$ and 180° are shown in Fig. 15. The absolute value of V_s is generally greater for $\psi=180°$ than for $\psi=0°$. Comparing the above result on velocities, Figs. 13~15, with the turned losses in Fig. 7, an important conclusion is deduced that the loss coefficient ζ is closely related with the absolute value of the secondary flow. Namely, when $\psi=180°$, the values of $\zeta=1.63$, 1.54, 1.34, and 1.38 correspond to the cases for the spacer length of $L=0$, 0.65 d, 4.7 d and 20 d respectively.

4·2·3 Three-dimensional double turns in different planes ($\psi=120°$)

Figure 16 gives a relationship between velocity profiles and the spacer length for $\psi=120°$, where it has nearly the greatest value. When the spacer is short, a very complicated flow is generated behind the elbows, due to a strong interference between two elbows. As an example, Fig. 17(a) shows an equi-velocity diagram at the section $L_d=0.8\,d$. Higher velocity regions exist on the lines O-A_1 and O-B_N, corresponding to the outside of curvature of the second elbow and inside of the first one. Flow patterns in Fig. 17(a) differ remarkably from those in Fig. 11. Velocity profiles V_s of the secondary flow at section $L_d=0.8\,d$ are shown in Fig. 17(b). Strong clockwise swirling motions are recognized on the diameters of A_P-B_P, A_1-B_1, and A_3-B_3. On the other hand, a pair of clockwise and counter-clockwise vortices, one on O-B_2 being strong and clockwise, and the other on O-A_2 weak and counter-clockwise, is generated on the line A_2-B_2. Position of the weak vortex roughly corresponds to region of lower velocity and that of the strong vortex to region of higher velocity.

The maximum value of the secondary flow velocity is seen to reach as high as 90 percent of the mean flow velocity. Validity of the results in Fig. 17(b) is carefully checked by measuring the velocity in many diametral directions. The flow picture of section $L_d=0.65\,d$ is nearly the same as that of section $L_d=0$, and decay of the secondary flow along the pipe line is shown for $L_m=0.65\,d$ in Fig. 18(a). A pair of vortices which have already existed at the upstream section $L_d=0.8\,d$ is reduced to a single vortex at section $L_d=3\,d$, a strong vortex absorbing a weak one. In this process, the axial velocity is uniformalized. Figs. 16 and 18. At section $L_d=6\,d$, the single vortex takes a nearly forced vortex form, which reduces to zero along the pipe line, maintaining the form. This vortex producing a strong loss extends as far as 160 d downstream from the second elbow. If this kind of vortex is generated in the suction pipe of a pump or a blower, the performance will considerably be changed. When L_m is longer than 10 d, this forced vortex is not generated, the reason being the same

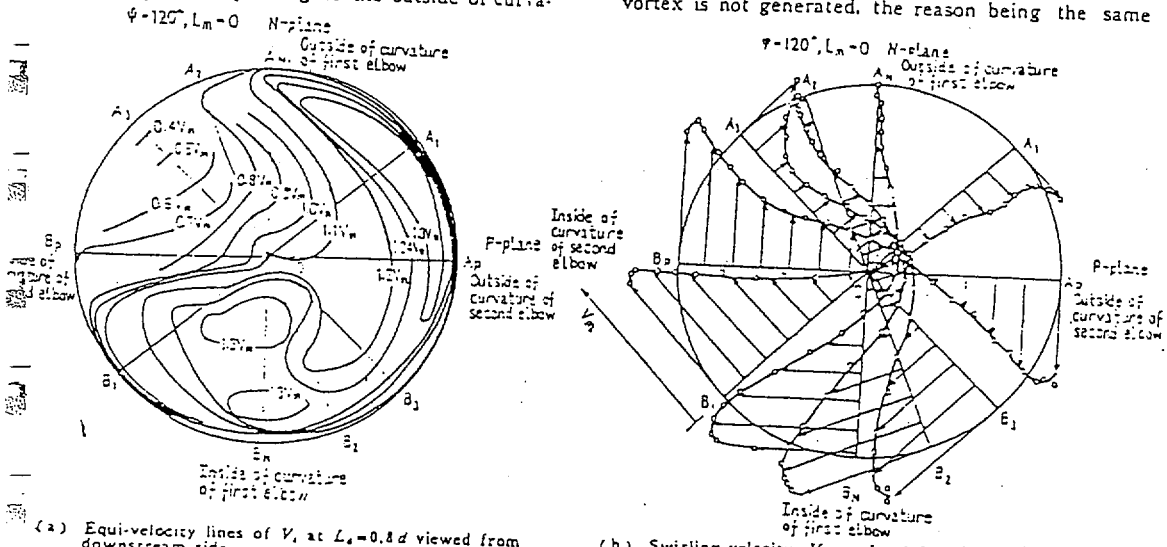

(a) Equi-velocity lines of V_s at $L_d=0.8\,d$ viewed from downstream side

(b) Swirling velocity, V_s, at $L_d=0.8\,d$ viewed from downstream side

Fig. 17

as given in section 4·2·2.

Figure 19 explains schematically the direction of vortex formation in a pipe downstream from the elbows. When water enters the second elbow with deformed flow conditions due to the first elbow, a centrifugal force acts in the second elbow as shown in the figure and a pair of strong and weak vortices is produced at the exit. The strong vortex absorbs the weak one and reduces to a single vortex, the sense coinciding to that of the strong vortex. Flow patterns for various bend conditions are shown diagrammatically in Fig. 20. The velocity profiles shown in pipe line correspond to the profiles on N-plane. The maximum velocity point is shown by a mark x. Arrowed solid lines represent the direction and the magnitude of flow velocity on the pipe centre. Arrowed dotted lines and broken lines illustrate those near both sides of pipe wall. The velocity profiles above pipe line show those viewed from the downstream side.

5. Conclusions

A pipe line is turned in various configurations with two right-angled elbows and the following results

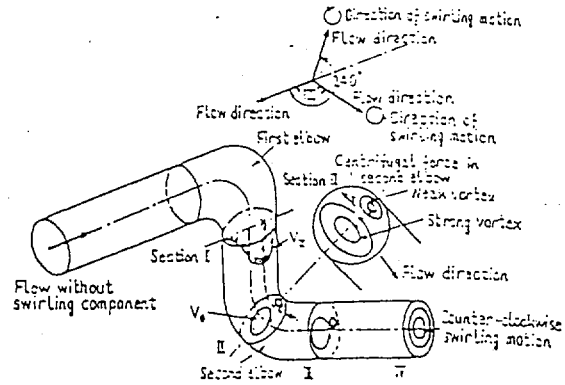

Fig. 19 Generation of swirling motion due to twisted pipe line

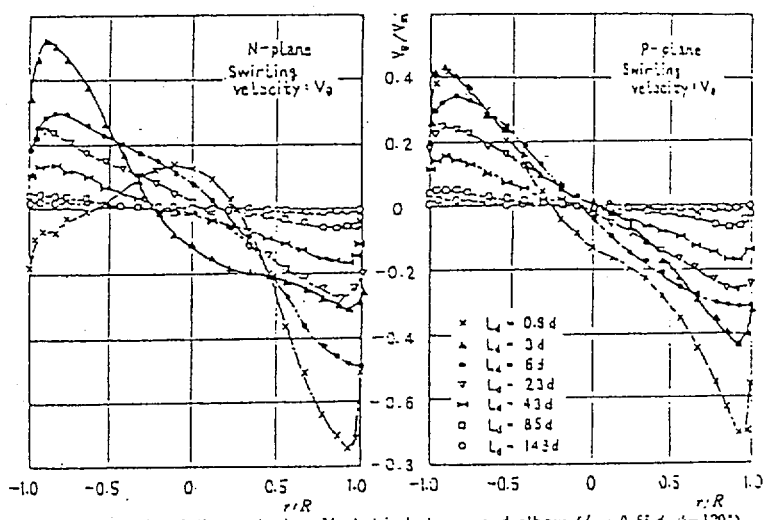

(a) Decay of swirling velocity, V_θ, behind the second elbow ($L_d = 0.65\,d$, $\phi = 120°$)

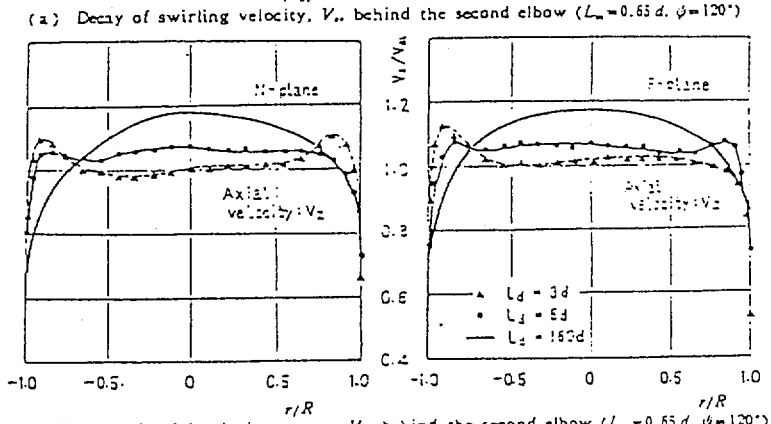

(b) Change of axial velocity curves, V_z, behind the second elbow ($L_d = 0.65\,d$, $\phi = 120°$)

Fig. 18

are obtained:

(1) When the spacer length L_m is less than $5d$, the elbows interfer each other intensively and the turned loss becomes minimum for $\psi=0°$, maximum for $\psi=120°\sim150°$, and medium for $\psi=180°$. When $L_m \leqq 0.65d$, the loss exceeds twice that due to a single elbow, and when $L_m=10d$, the loss becomes independent of the twisted angle of pipe line.

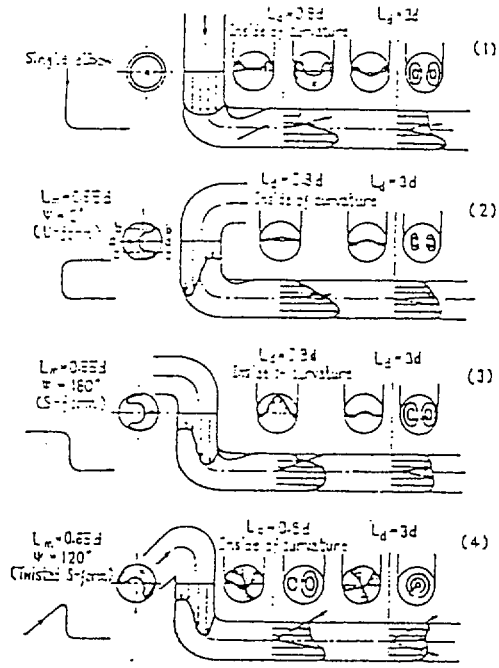

Fig. 20 Flow patterns for turned pipe line

(2) A secondary flow just behind a single elbow, $L_1=0.8d\sim3d$, shows an abnormal distribution, which recovers the normal condition at $L_2 \geqq 3$.

(3) With two elbows in the same plane, direction of a secondary flow behind the second elbow changes the sign when the spacer length L_m exceeds $2.15d\sim4.7d$.

(4) With two elbows in different planes, a forced type vortex is produced behind the bends when $L_m \leqq 4.7d$. The vortex becomes maximum at an angle $\psi=135°$ and it reaches about $135d$ downstream from the exit of the second elbow.

References

(1) W.R. Dean: *Phil. Mag.*, Vol. 4 (1927), p. 208.
(2) M. Adler: *Z. AMM.* Vol. 14 (1934), p. 257.
(3) R.W. Detra: *Mitt. E.T.H.*, No. 20 (1953), p. 1.
(4) H. Ito: *Trans. ASME*, Ser. D, Vol. 82, No. 1 (1960-3), p. 131.
(5) A.V. Saph and E.V. Schoder: *Trans. A.S.C.E.*, Vol. 47 (1902), p. 1.
(6) J. Eustice: *Proc. Roy. Soc. Lond.*, Ser. A, Vol. 85 (1911), p. 119.
(7) C.I. Corp and H.T. Hartwell: *Bull. Univ. Wisconsin*, No. 66 (1927), p. 1.
(8) C.M. White: *Proc. Roy. Soc. Lond.*, Ser. A, Vol. 123 (1929), p. 645.
(9) H. Nippert: *Forsch. Geb. Ing.-Wesen*, 320 (1929), S. 1.
(10) J.R. Henry: *NACA ARR*, L4F 26.
(11) Ito and Imai: Preprint of *Japan Soc. Mech. Engrs.*, No. 153, (1966-4), P. 81, (in Japanese).